

Integrated electro-optics on thin-film lithium niobate

Yaowen Hu^{1,2,*}, Di Zhu^{3,4}, Shengyuan Lu¹, Xinrui Zhu¹, Yunxiang Song¹, Dylan Renaud¹, Daniel Assumpcao¹, Rebecca Cheng¹, CJ Xin¹, Matthew Yeh¹, Hana Warner¹, Xiangwen Guo⁵, Amirhassan Shams-Ansari^{1,6}, David Barton^{1,7}, Neil Sinclair¹, and Marko Loncar^{1,*}

¹*John A. Paulson School of Engineering and Applied Sciences, Harvard University, Cambridge, MA 02138, USA*

²*State Key Laboratory for Mesoscopic Physics and Frontiers Science Center for Nano-optoelectronics, School of Physics, Peking University, Beijing 100871, China*

³*Department of Materials Science and Engineering, National University of Singapore, Singapore 117575, Singapore*

⁴*Institute of Materials Research and Engineering (IMRE), Agency for Science, Technology and Research (A*STAR), Singapore 138634, Singapore*

⁵*Department of Electrical and Computing Engineering, University of Virginia, Charlottesville, Virginia 22903, USA*

⁶*DRS Daylight Solutions, 16465 Via Esprillo, San Diego, CA, USA*

⁷*Department of Materials Science and Engineering, Northwestern University, Evanston, Illinois 60208, USA*

*Corresponding authors: yaowenhu@pku.edu.cn; loncar@seas.harvard.edu;

Electro-optics serves as the crucial bridge between electronics and photonics, unlocking a wide array of applications ranging from communications and computing to sensing and quantum information. Integrated electro-optics approaches in particular enable essential electronic high-speed control for photonics while offering substantial photonic parallelism for electronics. Recent strides in thin-film lithium niobate photonics have ushered revolutionary advancements in electro-optics. This technology not only offers the requisite strong electro-optic coupling but also boasts ultra-low optical loss and high microwave bandwidth. Further, its tight confinement and compatibility with nanofabrication allow for unprecedented reconfigurability and scalability, facilitating the creation of novel and intricate devices and systems that were once deemed nearly impossible in bulk systems. Building upon this platform, the field has witnessed the emergence of various groundbreaking electro-optic devices¹⁻¹² surpassing the current state of the art^{1-6,9-12}, and introducing functionalities that were previously non-existent^{3,7,8}. This technological leap forward provides a unique framework to explore various realms of physics as well, including photonic non-Hermitian synthetic dimensions¹³⁻¹⁵, active topological physics^{16,17}, and quantum electro-optics^{12,18-20}. In this review, we present the fundamental principles of electro-optics, drawing connections between fundamental science and the forefront of technology. We discuss the accomplishments and future prospects of integrated electro-optics, enabled by thin-film lithium niobate platform.

Introduction

Over the past century, photonic and electronic systems, both governed by the laws of electromagnetism, have become indispensable in advancing science and technology. The evolution of modern electronic systems, culminating in the creation of integrated circuits, has revolutionized our daily lives, influencing everything from computers and cell phones to automated control systems and robots. Simultaneously, integrated photonic systems offering broad bandwidth, minimal propagation loss, and massive parallelism, enabled by breakthroughs in micro- and nano-fabrication technologies have reshaped fields such as sensing, imaging, metrology, spectroscopy, and bio-medicine. At the intersection of these two dynamic fields is the field of electro-optics that harnesses distinct yet complementary properties of photons and electrons. On one end, electro-optics endows passive photonic systems with fast control provided by high-speed electronics, thus enabling modern communications^{21–25}, lidar^{26,27}, and optical coherent tomography^{28,29} systems. Conversely, photonics enriches electronics with the massively parallel processing capabilities, evident in advancements in photonic computing^{30–34} and microwave photonics^{35–39}, for example. These application-driven developments bridge the electronic and optical domains, leveraging materials that offer control of photons using electrical signals. While several physical mechanisms can be employed to achieve this, including thermo-optic, acousto-optic, free-carrier-dispersion, electro-absorption, and piezo-mechanic, the Pockels or EO effect, present in materials with $\chi^{(2)}$ nonlinearity, is a clear front-runner.

An ideal material platform for electro-optics necessitates a strong interaction between optical and electrical fields, along with minimal optical and electrical losses. It should also be amenable to microfabrication to construct advanced and highly complex systems in scalable fashion. While the quest for the material that meets these stringent criteria continues, the emerging thin-film lithium niobate (TFLN) photonic platform presents a compelling solution. Lithium niobate (LN), having played a pivotal role in optical technology for over seven decades, stands as a cornerstone in various technical applications and scientific disciplines. For instance, its use for optical phase and amplitude modulation has been a workhorse of modern communication technology, thanks to its impressive $\chi^{(2)}$ nonlinearity (~ 30 pm/V), high refractive index (~ 2.2), and wide transparency window ($0.4\text{--}5.5\ \mu\text{m}$). Its ability to be periodically poled also positions it as a crucial component for frequency conversion in nonlinear and quantum optics. Despite these remarkable properties of LN, its integration into complex chip-scale systems has historically been hindered by the absence of high-quality thin films and the difficulties associated with patterning this material. The recent commercialization of wafer-scale thin-film LN-on-insulator^{40–42} and the development of high-quality argon-based physical etching^{43,44} have ushered a new era of integrated electro-optics. These advancements have enabled nanoscale optical confinement resulting in enhanced EO interaction, while maintaining low optical losses. Brief yet storied history of the burgeoning field of TFLN photonics, has been detailed in several comprehensive reviews in Ref. ^{45–47}.

The essential component of TFLN electro-optics is the high-performance EO modulator: it allows electronic control of all degrees of freedom of light, including amplitude^{1,5}, phase⁴⁸, frequency³, and polarization state⁴⁹, as well as its temporal⁵⁰ and spatial profile⁵¹. TFLN-based modulators feature a very low half-wave voltage V_π (voltage required for a π phase shift of light, $\sim 1\text{V}$), low optical propagation loss ($\alpha \sim 1$ dB/m), and high EO bandwidth (BW ~ 100 GHz)^{1,5,43,52}. These attributes are the consequence of a strong EO interaction, long photon lifetime, and low microwave losses, respectively. In comparison to other photonic platforms, such as silicon and indium phosphide, which may excel in one or two metrics, the simultaneous achievement of these three attributes represents a substantial advantage of TFLN photonics. From a physics perspective, TFLN *enables the strongest coupling between optical and microwave modes, setting it apart from all other EO platforms*. From an application perspective, the combination of low V_π and high EO bandwidth results in an energy-

efficient and high-speed control. Meanwhile, minimal optical loss allows for the integration of many components and/or functionalities in series within the same circuit, allowing far more operations to be performed on light than any other platform, thus offering unprecedented system performance and capabilities.

Another important component of TFLN photonics are EO resonators, which can trap photons for periods of time (photon lifetime ~ 10 ns for cavities with quality factors $Q \sim 10^7$)⁴³. This duration significantly surpasses the operation time required to extract or inject the photon into and out of a cavity using the EO effect (~ 0.1 ns, Box 1), thereby allowing many EO operations to be performed within one photon lifetime. Furthermore, even more scientifically interesting and technologically pertinent functionalities emerge when two or more cavities are coupled together^{3,6-8,13,18-20}. Such configurations enable the interaction of multiple reconfigurable photonic energy levels through strong EO coupling, a feat nearly unattainable in their bulk counterparts. This advancement heralds a new generation of complex photonic devices and chip-scale systems (Box 1) that extend beyond the capabilities of traditional EO devices, which typically rely on EO modulation within a single waveguide and/or cavity. Moreover, combining the EO effect in TFLN with its inherent optical $\chi^{(2)}$ and/or $\chi^{(3)}$ nonlinearity, as well as piezoelectricity, offers many additional opportunities. These unique features on TFLN have underscored the need for more advanced mode-coupling formalisms in electro-optics, beyond the conventional formalism based on EO tensor and index change (Box 1).

This review aspires to present a comprehensive introduction to TFLN electro-optics, encompassing principles, formalisms, state-of-the-art technical developments, and applications. We hope this review will complement other reviews^{45-47,53-56}, which provide a broad overview of TFLN devices⁴⁵⁻⁴⁷, or are focused on nonlinear optics⁵³, and traditional EO modulators⁵⁴⁻⁵⁶. Thus, we hope our work will provide valuable insights into novel EO devices and systems on TFLN, and foster a deeper understanding in this rapidly advancing field. This is an exciting time for TFLN electro-optics, as it is transitioning from novel device-level demonstrations to advanced system level applications.

Basic principles of electro-optic modulation

EO (Pockels) effect

Electro-optics is the study of the interaction between electrical and optical fields through the EO effect. The most basic physical picture for the EO effect can be visualized as a static electric field inducing a constant change in the refractive index Δn of the material (Fig. 2a). The index change Δn is conventionally described using the electro-optic tensor R with element r_{ij} :

$$\begin{bmatrix} \Delta\left(\frac{1}{n^2}\right)_1 \\ \Delta\left(\frac{1}{n^2}\right)_2 \\ \Delta\left(\frac{1}{n^2}\right)_3 \\ \Delta\left(\frac{1}{n^2}\right)_4 \\ \Delta\left(\frac{1}{n^2}\right)_5 \\ \Delta\left(\frac{1}{n^2}\right)_6 \end{bmatrix} = R \begin{bmatrix} E_x \\ E_y \\ E_z \end{bmatrix} = \begin{bmatrix} r_{11} & r_{12} & r_{13} \\ r_{21} & r_{22} & r_{23} \\ r_{31} & r_{32} & r_{33} \\ r_{41} & r_{42} & r_{43} \\ r_{51} & r_{52} & r_{53} \\ r_{61} & r_{62} & r_{63} \end{bmatrix} \begin{bmatrix} E_x \\ E_y \\ E_z \end{bmatrix},$$

in which the $\Delta\left(\frac{1}{n^2}\right)_k$ with $k = 1, \dots, 6$ is the index change in the format of index ellipsoid in conventional nonlinear optics (see e.g. Ref⁵⁷ for details). Consequently, light propagating through this material undergoes an additional phase shift $\Delta\phi$ proportional to the index change Δn and the propagation distance L .

EO modulation

When a temporally varying electric field, for example a sinusoidal microwave signal, is applied, the induced phase shift $\Delta\phi$ oscillates with the amplitude of the microwave signal, resulting in the generation of new frequency components of light, with frequency intervals matching that of the microwave signal^{58,59}. This process, known as *EO modulation*, is a fundamental mechanism in electro-optics. Physically, the EO modulation involves the interaction of the microwave field with the optical field, where frequency of optical photons is changing through the absorption or emission of microwave photons. From an application standpoint, EO modulation serves as the bridge between microwave and optical domains, playing a pivotal role in the global optical communication network. For example, using this process, analog microwave signals can be imprinted on an optical carrier, as it is done in the fields of microwave photonics, or digital information can be encoded in both amplitude and phase of the optical signal, as it is done in optical communications. Conversely, optical signals with differing frequencies can interact via the EO effect, generating microwave signals that can be used to excite or control an electronic system.

A detailed formalism of EO modulation can be found in Box 1. Conventionally, the EO modulation is used to perform rapid modification of degrees of freedom of light such as temporal profile (e.g. by switching light on and off) and spectral content (e.g. by generating sidebands). In Box 1, we also discuss the mode-coupling formalism in which the EO modulation is represented as a coupling between different modes/energy levels and excites EO transitions of photons, which needs to be considered due to the strong EO coupling regime offered by TFLN.

TFLN photonics devices: cross section and material stack

In TFLN photonics, the basic device structures are the optical waveguides used to confine the light, and the electrodes to support the microwaves. The film of LN used to support such waveguides and electrodes are created via “smart cut” technology by slicing the bulk LN along a specific crystal axis (Fig. 2b). LN is birefringent material: it has two different refractive indices along different axis. Typically, the x and y axis have an ordinary refractive index n_o and z-axis has extraordinary index n_e . The largest EO tensor element is r_{33} (~ 31 pm/V), which requires applying the electric field along the crystal z-axis. Therefore, the electrode used to support the microwave field is designed to have the electrical field penetrating the slab along the z-axis of TFLN. The most commonly used films of LN can be classified into two types: x-cut and z-cut. The “x-cut” indicates that the thin-film of LN is precisely cut normal to the crystal x-axis, thus extending the film in the y-z plane of the LN crystal. Similar arguments apply to z-cut. In x-cut TFLN, the waveguide is ideally defined along the y-axis of LN, and parallel to it a pair of metal electrodes is introduced to form a capacitor, or for high-speed application a microwave transmission line (see Box 3 for microwave engineering of EO modulation). The signal and ground metal of the transmission line support an electrical field along the z-axis (Fig. 2c). This configuration may not be utilized nor possible in all designs, e.g. complex resonant structures, and in this case, only the field projection onto the z-axis contributes to effective modulation. In z-cut TFLN, the transmission line is designed so that the signal is on-top of the waveguide, leading to an electrical field perpendicular to the film plane (Fig. 2c).

Additionally, another viable option is the hybrid form of TFLN, which involves the creation of a waveguide through heterogenous film-bonding^{60–65} (Fig. 2c) or rib loading^{66–76} (see Fig. 2c). The hybrid TFLN platforms avoid etching LN, which alleviates concerns of possible Li⁺ contamination. This has led to extensive research on integrating TFLN with mature silicon and silicon nitride integrated photonics^{60–63,66–76}. Both chiplet/coupon-level^{60–63} and wafer-scale bonding of TFLN-on-Si or -SiN has been demonstrated^{64,65}. Recently, high-quality monocrystalline Si-LNOI wafers have also been demonstrated^{68,69}. These hybrid platforms typically have weaker mode confinement in the LN layer and therefore somewhat degraded EO efficiency. Nonetheless, with optimized mode engineering, state-of-the-art hybrid EO devices are exhibiting comparable performance to the monolithic ones that may already satisfy most practical applications^{4,60,77–79}.

While in this review we focus on monolithic (etched) x-cut TFLN waveguides, we note that our discussions and conclusions qualitatively apply to other system configurations.

Major classes of EO devices on TFLN

The three major classes of TFLN EO devices are those based on waveguides, cavities (resonators), and coupled cavities (Fig. 2d). The most fundamental structure is the waveguide-based phase modulator (PM)⁴⁸, which allows for precise phase control of the light passing through it. By placing one PM in each arm of an on-chip Mach-Zehnder interferometer (MZI), an amplitude modulator (AM) can be realized. This device leverages the interference between two paths that light can take to exert control over the amplitude of light^{1,4,5,52}. Single-cavity devices can be achieved by placing a PM inside a cavity^{2,14}. In this configuration, the phase change effectively alters the free spectral range (FSR) of the cavity, leading to a change of the frequency of the resonance. Note that the change of FSR due to EO effect is typically much smaller than the FSR itself, thereby in most of cases, only resonance frequency modulation is observed under an external phase modulation. Alternatively, one can embed an AM in a cavity, allowing control over the resonator's loss. It is worth noting that phase-modulated and amplitude-modulated cavities manipulate the real and imaginary components of the mode's energy. More advanced devices enabled by TFLN are coupled-cavity devices^{3,6,8,13}. They typically consist of two or more evanescently coupled cavities. Each cavity supports discrete modes – energy levels – each with its own loss or gain (e.g. from ion-doping or parametric gain). The advancement of coupled-cavity devices on TFLN lies in the EO modulation, which enables photonic EO transitions between different energy levels. These levels and their associated loss/gain are highly reconfigurable. Consequently, various coupled-cavity devices with new functionalities and high performance have been realized over the past several years. Section 3 discusses specific EO devices in more detail.

Fundamental rules for efficient electro-optic coupling/transition

While conventionally EO modulators are treated as switch/pulse generator in temporal domain or sideband generator in frequency domain, the EO modulation on TFLN for advanced EO devices/functionalities (e.g. cascaded frequency shifting, topological transport in cavity-based devices, EO frequency comb generations, EO synthetic dimensions, etc) can be more conveniently described as a process of EO coupling/transition between different modes (i.e. energy levels). The design of these systems using the EO mode-coupling formalism, should account for three fundamental rules: energy conservation, momentum conservation, and selection rules.

Energy Conservation. This rule is straightforward. For instance, if the input light is at a frequency ω_{L1} and the goal is to generate a frequency component ω_{L2} , a microwave signal with a frequency of $\omega_m = |\omega_{L2} - \omega_{L1}|$ is required. In the case of a resonant structure, for the modulation process to be efficient,

the frequencies ω_{L1} and ω_{L2} must also match the frequencies of the two individual resonant modes of the device, ω_1 and ω_2 .

Momentum Conservation. In all-optical three-wave mixing, the momentum conservation (also called phase matching) between three participating optical modes is an important consideration. In electro-optics, one of the optical modes is replaced with electromagnetic signal of a lower frequency, typically in the microwave range. Given the relatively long wavelength of microwaves (ranging from centimeters to millimeters), their momentum ($k_{MW} = 2\pi/\lambda_{MW}$) is typically small. As a result, the momentum conservation considerations are only relevant at high frequencies (>10 GHz) in which the k_{MW} is not negligible. Additionally, momentum conservation becomes significant only when travelling wave configuration is used for the microwave electrode (see Box 3 for details), as standing wave microwaves lack net momentum. Consequently, this momentum conservation effect is particularly relevant for waveguide-based traveling-wave EO modulators. It is worth noting that, in modulator design, this momentum consideration is often referred to as velocity matching (refer to Box 3 for details).

Selection Rule. Similar to atomic physics, where an atomic transition is only allowed when an external drive induces a non-zero off-diagonal coupling between the two states in the Hamiltonian, EO transitions adhere to a similar selection rule: there should be a non-zero overlap between the initial and final optical modes in the presence of an EO interaction. For instance, consider the photonic two-level system that is formed by a double-ring coupled-cavity (see Box 1 for details), of interest for realization of frequency shifters and beam splitters³, quantum transducers^{18,19}, etc. Here, EO modulation applied to the device can drive a transition between the two eigenmodes, in this case symmetric (S) and anti-symmetric (AS) modes. Note that the phase accumulation due to the EO effect on each ring needs to be different, in contrast to the same phase advance (or delay) on both rings, which will not create mode overlap between the S and AS modes via EO coupling. The same phase advance (or delay) only creates a global phase shift for the S or AS modes (see Box 1 for details). Another example is the cavity EO comb, which employs an EO-modulated racetrack-style cavity in the roundtrip resolved regime (see Box 1 for the definition of modulation regimes). This setup aims to establish coupling between modes separated by a cavity FSR. These different modes experience different overall phase accumulation after light makes one roundtrip in the cavity. Note that in the roundtrip-resolved regime that we define as $\omega_m \sim \text{FSR}$ or $\omega_m \gg \text{FSR}$, the microwaves cannot be regarded as unchanged during one roundtrip of light. Consequently, the electrode is designed such that, at a fixed point in time, the upper arm of the cavity has phase advance (delay) while the bottom arm has phase delay (advance). This configuration ensures that light experiences the same phase advance (or delay) in both arms because the sinusoidal microwave voltage reverses its sign after half a roundtrip. Thus, based on the specific functionality of the devices, the selection rule must be deliberately tailored to create mode-overlapping coupling and needs to be carefully considered for different modulation regimes.

Electro-optics enabled by thin-film lithium niobate

Phase and amplitude modulation

EO phase shifters/modulators are the simplest EO devices. They can be realized by passing a waveguide through a pair of electrodes^{80,81,48} (see Fig. 2a, b, c). Embedding PMs in an interferometer or resonator can implement an AM. The most widely used form of AM is the traveling-wave Mach-Zehnder modulator (MZM) (Fig. 2d, e, f), where the two arms of a Mach-Zehnder interferometer pass

through the two gaps of a coplanar waveguide (CPW) electrode¹. In a MZM, since the two arms experience opposite phase shifts, V_π is half of that of a phase modulator with the same length. Key FOMs of an EO modulator include insertion loss, half-wave voltage (V_π), EO bandwidth, linearity, and extinction ratio (only applicable for AMs). These FOM are interrelated, and tradeoffs exist. For instance, a smaller electrode gap reduces V_π but may increase metal-induced optical absorption; a longer modulator has smaller V_π but leads to smaller EO bandwidth due to microwave loss and possibly imperfect velocity matching. Overall, the EO performance largely depends on electrode design, in which velocity matching, impedance matching, and microwave loss are important considerations (see Box 3). A key advancement in improving the EO bandwidth is the adoption of capacitively loaded CPW electrodes^{52,82–84}, where microstructured segments are added in the CPW gaps. Doing so prevents current crowding on the edge and reduces microwave loss. One drawback is that the capacitive loading reduces the microwave phase velocity, which requires a low-index handle wafer (such as quartz⁵²) or undercuts in the high-index Si substrate⁸² to maintain velocity matching.

State-of-the-art TFLN MZMs have achieved V_π of ~ 1 V, extinction ratio > 20 dB, 3-dB bandwidth > 100 GHz, and total insertion loss of a few dB (including a large fiber-chip coupling loss and a sub-dB on-chip insertion loss)⁵. Combining two MZMs can realize an in-phase/quadrature (IQ) modulator⁸⁵ (Fig. 3g, h), an essential component for coherent communications. With a dual-polarization IQ modulator, a record-high single-wavelength data rate of 1.96 Tb/s was demonstrated^{5,86}. Some more recent developments include meander designs of long modulators^{87,88}, investigation of mm-wave operation⁸⁹, improved linearity using a ring-assisted Mach–Zehnder interferometer configuration⁹⁰ (Fig. 1i, j), and double-/multi-pass (or loop-back) phase modulators for RF V_π reduction (Fig. 1b, c) (see specific applications in Section “Waveguide-electro-optic frequency comb”)^{12,91}.

The transparency of LN at visible wavelengths renders TFLN modulators compatible with technologies ranging from bio- and environmental sensing to AR-VR and quantum information science and technology. Thanks to the wavelength dependence of the EO phase shift $\Delta\phi \sim \lambda^{-1}$ as well as the reduced waveguide-electrode gaps at shorter wavelengths^{10,11}, AMs with $V_\pi \cdot L$ s as low as 0.17 V·cm at 450 nm have been reported¹, with highest reported 3-dB bandwidths (~ 35 GHz) being limited only by the electrode design^{10,92}. Quantum applications of TFLN visible modulators have demonstrated, including scalable processing single photons from a deterministic quantum emitter⁹³ and photonic engines integrated with spatial light modulators for fast, free-space control of atomic systems⁹⁴.

As mentioned, the TFLN platform supports various micro- and nano-structures that allow more complex modulator designs to be implemented. This includes resonant modulators based on micro-rings^{3,95–97}, photonic crystals^{98,99}, as well as Bragg grating-based reflector or Fabry-Perot cavities^{100–102}. Resonant modulators have small footprint and low V_π , but high-Q resonances will limit their operating bandwidth. One potential resolution is to use a design where a ring resonator is coupled to the bus waveguide through an MZM, and modulation affects the coupling instead of shifting the resonance¹⁰³. Some other variations of EO modulators include Michelson-interferometer modulators^{104–106}, EO polarization controller¹⁰⁷, and compact slow-light MZMs¹⁰⁸.

TFLN modulators offers groundbreaking improvements over previous commercial lithium niobate modulators and devices on other material platforms (see details performance comparison in ref. ^{1,55}). Further improvements on the V_π , bandwidth, and insertion loss are possible by increasing the microwave-optical mode overlap, improving the optical loss, velocity matching, and microwave loss (see Box 3 for microwave engineering). Reducing the TFLN modulator size is crucial for large-scale electro-optic systems and are possible by folding the microwave electrode or exploring new types of modulators. With direct industrial applications, telecom-wavelength TFLN phase and amplitude modulators are experiencing rapid development, and the ever-expanding literature is difficult to fully

capture here. This section only intends to give a brief overview of some representative works and relatively recent progress. For a more thorough and detailed review on this specific topic, readers may refer to Refs. ^{45,55,56}.

Electro-optic frequency comb generation: waveguide-based

The EO frequency comb is generated by microwave driven modulators, resulting in sideband generation where each sideband represents one comb line. It offers electrical control over the comb dynamics and maintains intrinsic phase coherence among all comb lines. A comprehensive review on EO combs can be found in Ref. ¹⁰⁹. Traditional EO combs are typically waveguide-based. In this setup, light passes through a PM, and the output light can be expressed as $E_{out} = E_0 e^{i\omega_0 t - ikz} e^{i\beta \cos(\omega_m t + \phi)}$. The term $e^{i\beta \cos \omega_m t}$ is the generation function of a Bessel function. Therefore, one can directly expand $e^{i\beta \cos \omega_m t}$ to obtain the analytical solution for the output field: $E_{out} = E_0 e^{i\omega_0 t - ikz} \sum_n J_n(\beta) e^{in(\phi + \frac{\pi}{2})} e^{in\omega_m t}$. Building upon this, one can cascade several PMs or AMs together to obtain a broader waveguide EO comb¹¹⁰, in which the use of AMs flattened the comb shape.

The field of waveguide EO combs has been rapidly growing in recent years. Frequency combs with more than 40 spectral lines spanning 10 nm have been demonstrated using only a single PM⁴⁸ with $V_\pi = 3.5 - 4.5$ V at 5 – 40 GHz. A microwave driving power of ~ 3.1 W is used, corresponding to a modulation index $\beta \sim 4\pi$ ⁴⁸. Building upon this breakthrough, flat-top waveguide EO combs on TFLN were first demonstrated by cascading an AM with a PM, as shown by Yu et al⁹ and Xu et al¹¹¹. For example, in Yu et al⁹, a total of 67 comb lines with a 12.6 nm span were demonstrated by driving the device with 3.8 W microwave power. This work utilized a loop-back structure for the PM to reduce the V_π of the PM to 2 – 2.5 V. Loop-back geometry, however, creates a weak resonance that makes the V_π frequency dependent (multiples of ~ 3 GHz in frequency combs reported by Yu et al⁹). Although bulk system can achieve similar comb line number and spans, it requires a cascade of one AM with three PMs. TFLN waveguide EO combs significantly reduce the system complexity. One drawback of current EO combs is the need for multiple high power microwave sources. Addressing this challenge could be groundbreaking for waveguide EO combs. These combs are ideally suited for applications that require good spectral flatness and do not necessitate wide span, such as data communications.

Synthetic electro-optic crystal generation

The concept of a photonic synthetic dimension in the frequency domain is rooted in the arrangement of distinct optical frequencies to construct a lattice. Nonlinear processes, such as EO modulation, facilitating lattice coupling. This approach holds promise for simulating complex physical systems and exploring novel physics, due to the high frequency and wide bandwidth of light, along with reconfigurability, scalability, and the capability to control gain and loss. These attributes have enabled the exploration of non-Hermitian^{112,113}, high-dimensional^{14,114}, and topological systems¹¹⁵⁻¹¹⁹, to name some examples, as well as Moire lattices¹²⁰, which can be challenging to study using other methodologies. The simplest configuration of a synthetic EO crystal involves a single EO modulation applied to a cavity with microwave frequency equal to the FSR (Fig. 21). This is formalized by considering the EO cavity in the roundtrip resolved regime (see Box 1). Advanced structures that involve multiple modulation tones or coupled cavities can be extended in this formalism (see Box 1). Although simple in concept and geometry, this field has shown great potential and excellent experimental progress in fiber-optics systems¹¹³, but has been limited by scalability and high insertion loss challenges inherent to this approach. TFLN holds promise as a catalyst for advancing this field: the strong EO enables strong coupling rates and low loss between lattice points, orders of magnitude

beyond the loss rate of each lattice point (EO coupling $\Omega \sim 10$ GHz, optical loss rate $\kappa \sim 100$ MHz), a regime that is inaccessible for other photonic platforms. These features suggest large-scale and intricate synthetic crystals can be realized.

Recently, high-dimensional frequency crystals, extending up to four dimensions, were demonstrated using a single EO cavity on TFLN, in addition to measurement of density of states and a coherent random walk¹⁴ (Fig. 2m). Instead of folding a 1D lattice to achieve higher dimensionality, as is done conventionally^{119,121,122}, rather the high-dimensionality is achieved by using several different microwave drives with their frequencies closely matching (mutually detuned by 1 MHz) the cavity FSR (~ 10 GHz). As a result, each microwave drive provided an individual dimension for photons to hop, leading to each dimension encompassing over 100 lattice points. Furthermore, a crystal with a frequency domain mirror, i.e. a device capable of reflecting optical energy propagation along the frequency dimension, was proposed and experimentally demonstrated¹³. This was accomplished using both coupled-cavity and polarization crossing. The mirror exhibited a reflectivity exceeding 0.9999, showcasing interference of forward and backward waves, along with the observation of trapped states in the frequency domain. More recently, exploration of synthetic dimensions using TFLN has gone quantum and used to explore correlations between entangled photons and multilevel Rabi oscillations, in which quantum frequency conversion was employed to create a second dimension¹⁵.

Electro-optic frequency comb generation: cavity-based

The simplest configuration of a cavity EO comb involves placing a phase modulator (PM) inside a high-Q cavity. Light circulates within the cavity, passing through the PM multiple times, which, as discussed in Sec. 2 (selection rule), enables broadband EO comb generation. Tight confinement of the waveguide in TFLN, along with a high-performance PM, facilitates this configuration while maintaining a high-Q cavity. This is a significant advantage compared to bulk systems where the insertion loss of bulk components is typically large. The underlying mechanism of single-cavity EO combs can be modeled using roundtrip-resolved modulation (see Box 1 for details), the same model used to study EO synthetic crystals. In 2019, a single-cavity EO comb was successfully demonstrated on TFLN (Fig. 2h), achieving a span one order of magnitude larger than previous EO combs^{2,123}. However, despite this impressive span improvement, the conversion efficiency of this type of comb remains limited, approximately 0.3%⁶. The low conversion efficiency arises from the cavity becoming strongly under-coupled when driven with a strong microwave tone. The microwave drive introduces a broadband comb generation process, acting as an effective intrinsic loss κ_{MW} for the pump mode⁶. This behavior is analogous to the generation process for other types of frequency combs, such as Kerr combs. On TFLN, the effective loss rate due to the microwave drive (κ_{MW}) is about 100 times higher than the external (κ_e) and intrinsic (κ_i) loss rates of the cavity (i.e. $\kappa_{MW} \sim 10$ GHz, $\kappa_e \sim \kappa_i \sim 100$ MHz for ~ 1 million quality factor⁶). This means that $\kappa_e \gg \kappa_i + \kappa_{MW}$. Simply increasing the external coupling to achieve critical coupling with the microwave drive results in high loss for resonance modes, reducing the overall bandwidth.

This issue has been addressed by implementing the concept of GCC proposed in Ref. ³, and discussed more in the following section, to a coupled-resonator EO comb (Fig. 2g, i). This led to a 100-fold improvement in efficiency (30%) and a 2.2-fold improvement in span (132 nm)⁶. Another challenge with cavity EO combs is achieving a flat-top comb shape. Recent work has shown that a flat-top cavity EO comb can be achieved by using a boundary as a frequency domain mirror¹³ (see previous section). With the significant progress in TFLN-based cavity EO combs, it is anticipated that they will become valuable broadband and stable comb sources, enhancing applications in telecommunications, metrology, astronomy, spectroscopy, and more. It should be pointed out that, cavity-based EO comb has the limitation on the microwave power consumption as well as the tunability of the repetition rate

due to the resonant enhancement condition. TFLN has provided a versatile platform for cavity-based EO comb with novel structures, unlocking possibilities to further improving the bandwidth, conversion efficiency, and spectral flatness. Finally, it is important to note that, cavity-based EO comb also generates femtosecond pulse source⁶ as conventional EO comb, benefiting applications on ultrafast optics.

Frequency conversion: general critical coupling and photonic molecules

Microwave-enabled control of light holds a great promise for applications requiring ultrafast operations, such as frequency conversion, sensing, and switching, due to the compatibility with ultrafast electronics and the stability of microwave signals. However, this typically necessitates a photon lifetime significantly longer than the time required to transition between states, which was difficult to achieve in other photonic platforms. TFLN overcomes this limitation by simultaneously featuring strong EO coupling on the order of gigahertz, and high-Q cavities corresponding to low loss rates of 10-100 megahertz (as defined in Box 1). Consequently, TFLN now facilitates EO transitions between modes of different energy in both single and coupled cavities. For instance, within a single cavity, applying a microwave with a frequency equal to the FSR creates EO transitions across a synthetic frequency lattice. In a coupled-cavity system, microwaves can induce transitions between several hybrid modes, if energy conservation, phase matching, and selection rules are satisfied (as explained in the section on "rules for efficient electro-optic transition").

Recently, a photonic two-level system (TLS) with EO transition was demonstrated using two coupled-cavities on TFLN^{3,8} (Fig. 2a). This system can induce EO coupling (with $\Omega \sim 5$ gigahertz) between the S and AS modes of the coupled-cavity (see Box 1 and the selection rule in section 2), leading to Rabi oscillations between the two energy levels. As an optical TLS, this device is well-suited for GHz-scale frequency control, a critical energy band for communications and computing.

Typically, this EO coupling results in energy oscillations between the two frequencies, which is unsuitable for efficient energy conversion. To address this, the concept of general critical coupling (GCC) has been proposed for efficient energy conversion³ (see Box 2 for detailed introduction). Combining GCC with the TLS coupled to a continuum, e.g. a bus waveguide, enables novel EO frequency shifters and beam splitters (Fig. 2b). Record-breaking frequency shifting performance was demonstrated, with over 99% shift efficiency (shift ratio), 0.45 dB on-chip insertion loss, and a shift frequency range of 10-30 gigahertz, all achieved using only a continuous single-tone microwave³. Furthermore, a concept of cascaded frequency shifting is introduced, and a cascaded frequency shifter (a triple-coupled-cavity device) is demonstrated, achieving a four-step cascade to a 120-gigahertz frequency shift using a 30-gigahertz microwave³. Here, energy flows through a ladder of energy levels without any back reflection. This device showcases the potential to access energy bands exceeding 100 gigahertz using only a low-frequency microwave source. High-performance frequency shifting and beam splitting operations at GHz band have the potential to impact applications in communications^{21,124}, classical information processing^{35,39,125,126} as well as quantum computing¹²⁷⁻¹³². Finally, another type of triple-coupled-cavity system has been demonstrated, forming a three-level system⁷ (Fig. 2c), and was used to realize an optical isolator. Nearly 40 dB of optical isolation is achieved using approximately 75 milliwatts of microwave power. These novel EO transitions in coupled-cavity systems offer a fully reconfigurable photonic system with ultrafast control, revitalizing the applications of EO systems. Further increasing the mode overlap and the cavity quality factor can significantly improve the coupling regime and extending to large-scale EO cavity array can enable advanced complex system with collective dynamics.

Frequency conversion: spectral shearing

Electro-optic spectral shearing is another approach for altering the frequency of light. It enables a substantial shift in frequency, typically on the order of ~100 GHz, and requires only a single-tone microwave driving signal. The underlying principle of spectral shearing lies in the fact that a linearly ramped phase modulation $\Delta\phi = kt$ is equivalent to a frequency shift of light: $E_{out} = E_{in}e^{ikt} = E_0e^{i\omega_0t - ikz}e^{ikt} = E_0e^{-ikz}e^{i(\omega_0+k)t}$. It's important to note that while spectral shearing can achieve a very large frequency shift beyond the microwave driving frequency (in the case of sinusoidal microwave drive), it only works for pulsed light. The duration of pulse needs to be shorter than the linearly rising (or falling) part of the sinewave. When using a sinusoidal modulation, the phase modulation applied $\Delta\phi = \beta \sin(\omega_m t + \Delta\varphi) \approx \beta \omega_m t \cos \Delta\varphi$, in which $\Delta\varphi$ is the relative phase between the microwave and optical pulse, ω_m is the microwave frequency, and β is the modulation index (see Box 1 for definition)¹². Here, the frequency shift $\Delta f = k = \beta \omega_m \cos \Delta\varphi$ of the linear ramping phase represents the magnitude of the frequency shift and is determined by the peak-to-peak voltage and the frequency of the used sinusoidal signal¹². An important figure of merit is the effective shift magnitude ($\Delta f / \delta f$) that is defined as a ratio between the frequency shift that can be achieved Δf and the bandwidth of optical pulse δf . Consequently, increasing the frequency of the modulation signal to obtain a larger Δf (since $\Delta f \propto \beta \omega_m$) does not necessarily help the $\Delta f / \delta f$. Higher frequency modulation leads to shorter periods, necessitating shorter pulse durations (i.e., higher pulse bandwidth δf). As a result, the ultimate limit on the $\Delta f / \delta f$ determined by the amplitude of the applied phase modulation, which is constrained by the V_π of the phase modulator. Note that serrodyne (i.e. sawtooth) modulation^{133,134}, in which the voltage is repeatedly linearly ramped, mitigates the bandwidth constraint but the required high-bandwidth microwave signal is difficult to achieve, even with high-bandwidth modulators.

Spectral shearing has been successfully demonstrated in bulk systems^{135,136} and employed in quantum applications but typically has limited $\Delta f / \delta f < 1$ with $\Delta f \sim 200$ GHz, due to the high V_π of bulk modulators. On TFLN, spectral shearing of single photons with a shift frequency of $\Delta f = \pm 641$ GHz (± 5.2 nm) has been achieved¹², resulting in an $\Delta f / \delta f$ greater than 1. Furthermore, an impressive 8-fold suppression of pulse bandwidth (from 6.55 nm to 0.35 nm) has been demonstrated by applying quadrature phase modulation using the same device. With sub-volt TFLN at visible wavelengths, a spectral shearing with a $\Delta f / \delta f > 7$ has been achieved with $\Delta f = 6$ GHz¹⁰.

Cryogenic electro-optics

The EO effect in TFLN persist at cryogenic temperatures, as well. This offers an effective solution for realizing photonic links for superconducting microwave circuits¹³⁷ or for on-chip optical routing and processing for optically active ions or defects in the solid-state. Superconducting devices, such as qubits, logic circuits, and detectors, rely on cryogenic operation. As systems scale up, the RF cables required to address these devices will induce unmanageable heat load to the host cryostats. In addition, for constructing a quantum network that connects distant superconducting qubits, direct transmission of microwave photons through RF cables at room temperature is infeasible due to microwave loss and thermal noise. A promising solution is to replace metallic cables with optical fibers, which have low thermal conductivity and are wide bandwidth (THz) and ultra-low loss (< 0.2 dB/km) optical channels. Central to this solution is an efficient and cryogenically compatible mechanism to transduce between microwave and optical signals. Combining a TFLN EO modulator with superconducting electrodes provides a viable solution.

One approach to achieve an ultra-efficient cryogenic EO interface is to use cavity systems^{138–140}. This scheme, referred to as cavity EO, is suitable for coherent, bidirectional microwave-optical quantum transduction^{141,142}. On TFLN, it can be implemented by replacing the electrode of a double-ring coupled-cavity modulator with a superconducting resonator (Fig. 2d, e, f), with a resonance frequency matching the doublet splitting of the S and AS optical modes (see Box 1 for details)^{18–20}. A strong laser pump at the red mode can upconvert a microwave photon into an optical photon at the blue mode. In cavity EO system, the key FOM is the cooperativity, $C = 4g_0^2 n_p / \kappa_m \kappa_o$, which depends on the EO interaction strength g_0 , microwave loss κ_m , optical loss κ_o , as well as the number of pump photons n_p that can be put into the system without inducing quasiparticles in the superconductor, creating noise photons, or overheating the cryostat^{142,143}. State-of-the-art cavity EO transduction on TFLN has achieved an efficiency of 1.02% (internal efficiency of 15.2%)²⁰. Further improvement requires microwave and optical cavities with higher quality factors, as well as better optical coupling and cryogenic packaging. It is worth mentioning that even with low efficiency, cavity EO transducers can enable heralded entanglement between distant superconducting systems¹⁴⁴. Pumping the cavity EO device at the blue hybrid mode can generate pairs of microwave and optical photons via spontaneous parametric down conversion. The optical photons can be sent to a distant location to establish entanglement with another pair source through the DLCZ protocol. Similarly, difference frequency generation between two optical fields can be used to generate microwave signals inside the cryogenic environment, that can be used to control superconducting qubits¹⁴⁵.

Cavity systems enhance EO interaction at the expense of operating bandwidth. For applications such as rapid single flux quantum (RSFQ) circuits, superconducting nanowire single-photon detectors, and frequency-multiplexed superconducting qubits, a broadband, low V_π modulator is desired. This can be achieved using a long traveling-wave modulator with superconducting electrode, which has negligible ohmic loss and breaks the tradeoff between length and EO bandwidth. Recently, a superconducting (niobium) TFLN MZM with effective modulation length of 1 m and a V_π as low as 42 mV was demonstrated. Such device (a 20-cm-effective-length device with 230 mV V_π and 17 GHz bandwidth) is used to transmit RSFQ signals (5 mV V_{pp}) at 4 K to room temperature through telecom optical fibers¹⁴⁶.

Emerging applications

With the recent rapid advancements in EO devices on TFLN, the field is transitioning from focusing on individual devices to comprehensive system-on-a-chip approaches. While there are many expected applications of this platform, including those in telecom, datacom, and microwave photonics, here we focus on several emerging applications and future opportunities.

Photonic computing and accelerators

Tightly integrated and power-efficient electronic and photonic systems can enable important advances and push the state of the art in optical communication systems. Furthermore, we envision such an integrated electronic-photonic system using TFLN will enable breakthroughs in optical computing as well as microwave photonics. With rapid advancements in AI and development of deep neural networks, CPUs and GPUs alike are challenged by impending bottlenecks in memory and speed while maintaining small form factor and low power consumption. Recently, the photonics community responded to these challenges with novel architectures, specialized towards accelerating the training and inference stages of such networks. The pioneering work of Shen et al. demonstrated audio recognition using a silicon-photonic chip¹⁴⁷. Following this demonstration, many photonic neural

network accelerators emerged, including processors based on frequency combs¹⁴⁸, phase-change materials¹⁴⁹, current-controllable optical attenuators¹⁵⁰, Mach-Zehnder interferometer meshes¹⁵¹, vertical-cavity surface-emitting laser arrays¹⁵², optical diffraction¹⁵³, and in combination with communications¹⁵⁴, further pushing the boundaries of computational accuracy, speed, and power consumption. Recognizing the impact, the TFLN platform promises to provide orders-of-magnitude advantages in aspects of speed and power consumption, and might play a key role in finally bringing photonic neural networks to market. The heterogeneous integration of lasers^{155–165} on TFLN provides high-power data channels, while EO^{2,6,123} and Kerr^{166–168} frequency combs provide potential for massively parallel frequency-division multiplexing across hundreds of channels. In each channel, high-speed EO modulators operating at CMOS-compatible voltages^{1,4,5} provide unprecedented levels of computational power and reconfigurability due to the analog nature of optical processing, in addition to efficiently encoding and manipulating data with ultra-low power consumption. Finally, the native $\chi^{(2)}$ nonlinearity coupled with high-speed integrated III-V photodiodes^{164,169,170} presents opportunity for on-chip nonlinear activation and opto-electronic conversion and detection, closing the loop for all-optical computation. As TFLN continues to mature in the coming years, we might just witness a fully monolithic photonic neural network competitive or even outclassing conventional electronic approaches.

Quantum photonics

The TFLN platform will play an important role in quantum photonics. The high carrier frequency of light allows both high-bandwidth quantum communication and, since this energy is far above the thermal background, the measurement of quantum states of individual photons^{171–174}. The properties of TFLN, including low-loss, possibility of large scale integration, possibility for photon-photon interactions through EO and/or optical $\chi^{(2)}$, render it an attractive platform for generating and manipulating quantum states of light¹⁷⁵. Although a single photon nonlinearity is not currently efficient in TFLN¹⁷⁶, the possibility of beam splitting and high-bandwidth EO phase shifting renders it attractive for linear-optical quantum computing¹³². Moreover, combs and modulators allow for such computing protocols in the frequency domain^{50,127–131,177–183}, taking advantage of the multiplexing ability of light. Indeed, the coupled ring system³ offers frequency-domain beam splitting without expanding the Hilbert space to using a single phase modulator¹⁸⁴. High-bandwidth switching offered by TFLN is also a key ingredient for rendering inefficient spatially multiplexed heralded states to be quasi-deterministic, which can be applied to photon sources and quantum communications^{185–187}.

The all-optical $\chi^{(2)}$ interactions on TFLN, often performed using periodic poling of TFLN¹⁸⁸, further enhances the EO platform. For example, it can be used for photon pair generation, squeezed light generation, and deterministic wavelength conversion of individual photons. These are of interest for photonic quantum computing, realization of quantum interconnects between devices that operate at different energy scales, up-conversion detection^{189,190}, quantum sensing and computing using highly squeezed states^{191–193}, and realization of efficient frequency combs via cascaded $\chi^{(2)}$ interactions¹⁹⁴. Beyond EO and $\chi^{(2)}$, the piezoelectric coupling of TFLN has been harnessed for quantum interconnects between microwave photons and acoustic phonons, with applications in, for instance, transduction or acoustic modulators¹⁹⁵. Furthermore, TFLN offers embedded rare earth ions¹⁹⁶, which promise quantum emitters, storage, signal manipulation¹⁹⁷, and sensors in addition to the depth of functionalities offered by TFLN itself. Overall, the depth of impact that TFLN has on quantum photonics with electro-optics is tremendous, and only recently we have begun exploring the potential of its impact.

Active topological photonics and non-Hermitian physics

Microwave-coupled optical lattices in frequency domain realized on TFLN^{3,6,7,13,18,19} are emerging as a promising platform for studying topological photonics, non-Hermitian physics, and microcavity sensing, for example. Combining TFLN with microcavity sensing^{198,199} is particularly promising for sensors that are both high-speed and highly sensitive. With the inherent strong piezoelectric interaction on TFLN, EO modulation could add a new control of degree of freedom to conventional acoustic sensors^{198,199}. Moreover, EO modulation on TFLN may enable the practical implementations of modulation-induced gauge field for photons²⁰⁰. Collectively, these advancements underscores TFLN's unique value in offering additional degrees of freedom for ultrafast tuning for various optical systems, making it an ideal platform for studying optical physics using waveguide and cavities and forging new directions for the manipulation and study of light.

Nonlinear photonics

The excellent $\chi^{(2)}$ and $\chi^{(3)}$ nonlinearities of TFLN allow parametric frequency-conversion processes to be combined with electro-optics, opening multiple opportunities for exploring fundamental physics, developing novel devices, and addressing practical applications. From physics perspective, the combined $\chi^{(3)}$ -EO⁶ and $\chi^{(2)}$ -EO^{15,201} introduces extra degrees of freedom and interactions for synthetic EO lattice. For example, the coexistence of EO and Kerr effect^{6,202} indicates the feasibility of introducing the on-site nonlinear interactions via Kerr effect in the synthetic EO lattice. This allows for the simulation of strong-correlated condensed matter models beyond the single electron approximation. From an applications standing point, integrated nonlinear frequency combs are particularly noteworthy, covering applications such as tunable optical parametric oscillators^{201,203,204}, ultra-stable microwave^{205,206} and millimetre-wave generation²⁰⁷, optical frequency referencing^{208,209} and synthesis²¹⁰, astrocomb^{211,212}, and ranging^{26,213}. The potential of integrated nonlinear frequency combs is set to expand by leveraging the multiple strong nonlinearities on TFLN. For example, at device level, TFLN facilitates novel comb generation that may harness the best properties of EO and Kerr effect, such as EO-Kerr comb in the same resonator⁶, EO-tunable Kerr combs²¹⁴, and cascading EO modulators with Kerr resonators²¹⁵. At system level, the combination of comb sources, modulators, and periodically poled lithium niobate waveguides can benefit these applications. Furthermore, the integration of new gain technologies such as the reflective semiconductor optical amplifier¹⁵⁷ and ion-embedding methods such as Erbium-doping of TFLN²¹⁶⁻²¹⁸ and Thulium-doped cladding oxides²¹⁹, with TFLN is promising. It may lead to exciting avenues in integrated lasers¹⁵⁵⁻¹⁶⁵ at exotic wavelengths and ultrafast, high peak power pulse generators²²⁰ and amplifiers^{219,221}. Such advancements may promise the deployment of chips for atomic physics at visible and near-UV²²², fully integrated supercontinuum generation²²³, and biomedical imaging²²⁴.

In this review, we have discussed the basic principles and formalisms of electro-optics on TFLN and introduced key research topics in this field. Electro-optics on TFLN has been developed tremendously over the past five years. It is unfolding as one of the most promising solutions for the next-generation of EO interfaces, such as the field of optical communications, microwave photonics, and photonic computing, where efficient and high-bandwidth EO conversion are paramount. It has the potential to continue providing revolutionary EO devices and circuits as well as hybrid circuits that interface with all-optical nonlinearities and acousto-optic interactions. As it matures, we expect TFLN to become one of the most important platforms of integrated photonics.

Acknowledgement

This work is supported by: Army Research Office/Dept of the Army (MIT) W911NF1810432; Air Force Office of Scientific Research FA9550-19-1-0376; Office of Naval Research N00014-20-1-2425; Air Force Office of Scientific Research (MIT); FA9550-20-1-01015; NIH/NEI (MGH) 5R21EY031895-02; Defense Advanced Research Projects Agency HR001120C0137; National Science Foundation EEC-1941583; Air Force Research Laboratory (Rigetti) FA864921P0781; Office of Naval Research (Vector Atomic) N00014-22-C-1041; National Science Foundation OMA-2137723; NSF (U Oregon) 2138068; NASA (U Oregon) 80NSSC22K0262; Department of the Navy (MAGiQ); NASA (ICARUS) 80NSSC23PB442; Air Force Office of Scientific Research (MURI UCB) FA9550-23-1-0333; National Research Foundation of Korea; Amazon Web Services Award number A50791; Harvard , FY 22 Spring Dean's Competitive Fund for Promising Scholarship; A*STAR (C230917005) and NRF (NRF2022-QEP2-01-P07, NRF-NRFF15-2023-0005); National Science Foundation Graduate Research Fellowship under Grant No. DGE-1745303

Box 1 Formalism of electro-optic modulation

The emergence of TFLN has expanded the landscape of EO devices, including single-cavity- and coupled-cavity-based configurations in addition to the conventional waveguide-based devices. These devices support many resonant modes with distinct frequency/ energy, that can be coupled via EO effect. This process of EO coupling can be understood as removing and/or adding photons from/ to a particular energy level (mode). Typically, the coupling strength Ω induced by EO effect is on the order of $\sim 1-10$ GHz^{3,6}, corresponding to an operation time of ~ 0.1 ns. This is much shorter than the cavity life time that can be routinely achieved in TFLN, that is on the order of $\sim 1-10$ ns for resonant modes with quality factor from 10^6 to 10^7 . This unique combination of large EO coupling strength (i.e. short coupling time) and ultra-low loss (i.e. large photon lifetime) supported by TFLN offers a fertile playground to explore numerous physical phenomena. This proliferation necessitates the development of new formalisms to accurately describe and analyze these increasingly intricate systems. In this section, we will first introduce the conventional formalism used to study EO effect, and subsequently discuss a recently developed approach based on mode-coupling.

Conventional approach

The traditional formalism to treat the EO process in LN has been used extensively in the field of nonlinear optics^{45,109}. It is based on the concept that an applied voltage introduces a phase shift to the optical field $\Delta\phi = \beta = \pi \frac{V}{V_\pi}$, where V_π represents the voltage required for a π phase shift. The term β is referred to as the modulation index or modulation depth. It is used to quantify the magnitude of the phase shift, essentially indicating how many π phase shifts are induced by the applied voltage. Consequently, light transmitted through a waveguide phase modulator, subject to a modulation signal $V_{mod} = V \cos(\omega_m t + \varphi)$, acquires a phase term: $E_{out} = E_{in} e^{i\beta \cos(\omega_m t + \varphi)}$, which can be expanded by Bessel function: $E_{out} = E_{in} \sum_n J_n(\beta) e^{in(\phi + \frac{\pi}{2})} e^{in\omega_m t}$. While conceptually simple, this formalism has complicated description when dealing with systems involves multiple spatial and frequency modes coupled together (e.g. multi-coupled waveguides or cavities with EO modulations), structures/regimes recently achievable on TFLN.

Mode-coupling approach

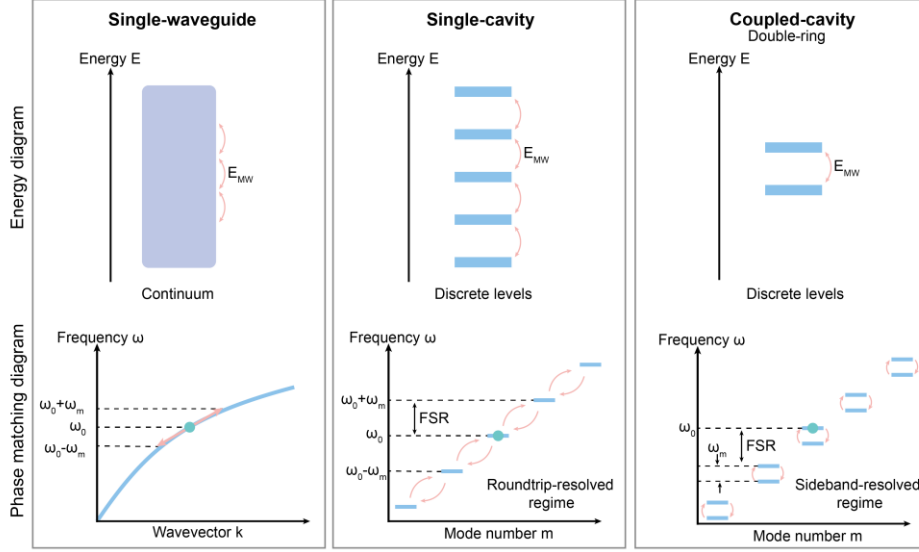
In contrast to using index change to represent the phase shift, the mode-coupling approach considers modulation as a coupling mechanism between frequency modes and involves an analysis of the system's Hamiltonian. Here we discuss the mode-coupling approach for three basic photonic structures: *single cavity*, *coupled cavity*, and *waveguide*.

1. Modulation in a single cavity.

When it comes to modulation within a single cavity, it is essential to recognize three distinct regimes that require separate considerations. They are defined as follows:

- **Sideband unresolved regime:** $\omega_m < \kappa$, when modulation frequency is smaller than linewidth of the mode.
- **Sideband resolved regime:** $\omega_m > \kappa$ but $\omega_m \ll \text{FSR}$, that is modulation frequency is larger than linewidth but much smaller than the FSR of the cavity.
- **Roundtrip resolved regime:** $\omega_m \sim \text{FSR}$ or $\omega_m > \text{FSR}$, modulation frequency is comparable with or larger than the FSR of the cavity.

In the case of TFLN, the ultrahigh quality factor resonances typically have MHz-level linewidths that is much smaller than typical modulation frequency that can be applied typically in GHz range. Consequently, we will focus our discussion on the sideband resolved regime and roundtrip resolved regime, only.



Box Figure 1 | Energy diagram and phase matching diagram for single-waveguide, single-cavity, and coupled-cavity systems with microwave modulation under different modulation regimes. ω_m , frequency of microwave; E_{MW} , energy of microwave photon; FSR, free spectral range. Green dot represents an actual optical photon.

In the **sideband resolved regime**, a cavity incorporating a phase modulator undergoes frequency modulation, expressed as $\omega_0 + \Omega \cos \omega_m t$. This configuration yields the Hamiltonian:

$$H = \omega_0 a_0^\dagger a_0 + (\Omega \cos \omega_m t) a_0^\dagger a_0$$

In which $\Omega = G_V \times V$ represents the EO coupling strength introduced by the microwave, a_0 is the cavity eigenmode with frequency ω_0 , and V is the peak voltage of the microwave drive. The factor G_V (approximately 0.5 GHz/V in TFLN) is related to the V_π of the modulator. It characterizes the frequency shift of the resonance when a 1V DC voltage is applied. Utilizing the Heisenberg-Langevin equation, the equation of motion can be derived as: $\dot{a}_0 = \left(-i\omega_0 - \frac{\kappa}{2}\right) a_0 - i(\Omega \cos \omega_m t) a_0 - \sqrt{\kappa_e} a_{in} e^{-i\omega_L t}$, where $a_{in} e^{-i\omega_L t}$ represents the pump field, a_0 denotes the cavity pump mode, ω_0 is the cavity resonance frequency, $\kappa = \kappa_e + \kappa_i$ corresponds to the cavity linewidth, with κ_e being the external coupling between cavity and bus waveguide, and κ_i signifying the intrinsic loss rate of the cavity. The output field from the bus waveguide is described by $a_{out} = a_{in} e^{-i\omega_L t} + \sqrt{\kappa_e} a_0$.

In the **roundtrip resolved regime**, where the modulation period ($1/\omega_m$) is comparable to the roundtrip time ($1/\text{FSR}$), the cavity's behavior cannot be simplistically viewed as frequency modulation. This is because the concept of cavity frequency is established through the roundtrip interference effect. In this scenario, the EO coupling directly affects a set of optical modes $\{a_n\}$ ($n = -N, \dots, N$ with $2N+1$ being the total number of modes considered) separated by the FSR. The Hamiltonian is given by:

$$H = \sum_{n=-N}^N \omega_n a_n^\dagger a_n + (\Omega \cos \omega_m t) (a_n a_{n+1}^\dagger + a_n^\dagger a_{n+1})$$

One can derive the equation of motion for $\{a_n\}$: $\dot{a}_n = \left(-i\omega_n - \frac{\kappa}{2}\right) a_n - i\Omega \cos \omega_m t (a_{n+1} + a_{n-1}) - \sqrt{\kappa_e} a_{in} e^{-i\omega_L t} \delta_{n,0}$. Details of solving such systems can be found in ref. ⁶.

It is worth noting that, in conventional approach, the coupling coefficient k between waveguide and cavity, roundtrip loss α , modulation index β are all unitless, while the κ_e , κ_i , and Ω is in the unit of hertz in the Hamiltonian. The relationship between these is $k = 2\pi \frac{\kappa_e}{\text{FSR}}$, $\alpha = 2\pi \frac{\kappa_i}{\text{FSR}}$, $\beta = 2\pi \frac{\Omega}{\text{FSR}}$ (e.g. $\kappa_e = 2\pi \times 100$ MHz, $\text{FSR} = 2\pi \times 10$ GHz $\rightarrow k = 0.06$)⁶.

2. Modulation in a coupled cavity.

For simplicity here we discuss the case of two coupled cavities with applied modulation in sideband resolved regime (Fig. 3a). More intricate configurations of coupled-cavity structures typically build upon or combine elements from this foundational case or incorporate the modulation in the roundtrip resolved regime. The Hamiltonian describing two coupled cavities in the sideband resolved regime is given by: $H = (\omega_0 + \Omega \cos \omega_m t) a_1^\dagger a_1 + (\omega_0 - \Omega \cos \omega_m t) a_2^\dagger a_2 + \mu(a_1^\dagger a_2 + a_1 a_2^\dagger)$, in which μ represents the strength of the evanescent coupling between two rings. This system can be simplified by applying a basis transformation: $c_1 = (a_1 + a_2)/\sqrt{2}$ and $c_2 = (a_1 - a_2)/\sqrt{2}$. In contrast, this yields a Hamiltonian akin to a photonic two-level system, with an interaction term analogous to Rabi oscillation:

$$H = \omega_1 c_1^\dagger c_1 + \omega_2 c_2^\dagger c_2 + \Omega \cos \omega_m t (c_1^\dagger c_2 + c_1 c_2^\dagger)$$

where $\omega_1 = \omega_0 - \mu$ and $\omega_2 = \omega_0 + \mu$. If both phase advance (or delay) is applied on a_1 and a_2 , it only creates a global phase at c_1 or c_2 . One can see that two ring with different phase direction changes ($a_1 + a_2$) towards ($a_1 - a_2$) and vice versa, thus satisfy the selection rule. Details of solving such a system can be found in the Methods of ref. ³. It is worth noting that only one ring is coupled to the waveguide, therefore the output field is $a_{out} = a_{in} + \sqrt{\kappa_e} a_1 = a_{in} + \sqrt{\kappa_e} \frac{1}{\sqrt{2}} (c_1 + c_2)$.

3. Modulation in waveguide.

In the waveguide, the spatial dimension z along the propagation direction assumes the role of time in the equation governing the EO-modulated cavity. For light $a_0 e^{i\omega_L t - ikz}$ with frequency ω_L passing through a single waveguide phase modulator, it gradually couples to other frequency modes a_n with frequencies $\omega_0 + n\omega_m$ ($n = \dots, -1, 0, 1, \dots$) as it propagates along the phase modulator:

$$\frac{d}{dz} a_n e^{ik_n z - i\omega_n t} = -i\Omega \cos(\omega_m t - k_m z) (a_{n-1} e^{ik_{n-1} z - i\omega_{n-1} t} + a_{n+1} e^{ik_{n+1} z - i\omega_{n+1} t})$$

Similar techniques involving the rotating frame can be employed to solve these equations. It is important to note that this represents a traveling optical wave in a waveguide, where phase matching considerations come into play as indicated by this equation.

Box 2 General critical coupling for efficient energy transfer

In optical systems, resonant modes with critical coupling conditions are commonly employed to enhance optical interactions (i.e., waveguide-cavity external coupling $\kappa_e =$ intrinsic loss κ_i). Nevertheless, in intricate optical systems, there may be multiple loss channels beyond the external and intrinsic losses. In particular, some optical mechanisms could serve as a loss channel for specific modes (e.g., the comb generation process acting as a loss channel for the pump mode, as energy is extracted from the pump and converted into the comb). Consequently, to facilitate efficient energy transfer and manipulate energy flow, it becomes essential to incorporate the concept of general critical coupling (GCC). Within this framework, in addition to the conventional losses stemming from coupling to the continuum (κ_e due to coupling to waveguide, κ_i due to scattering to environment), coupling to the resonant mode also introduces an effective loss.

This process can be modeled as a two-level system problem, in which one resonant mode a has conventional κ_e and κ_i and a second mode b with total loss rate γ is coupled to a through an interaction with coupling strength μ (this μ can be evanescent coupling between two rings, EO transition from microwave drive, or nonlinear interaction such as second harmonic generation). This process can be modeled as

$$\begin{aligned}\dot{a} &= \left(-i\Delta_a - \frac{\kappa_{e,a} + \kappa_{i,a}}{2}\right)a - i\mu b - \sqrt{\kappa_{e,a}}a_{in} \\ \dot{b} &= \left(-i\Delta_b - \frac{\kappa_b}{2}\right)b - i\mu a\end{aligned}$$

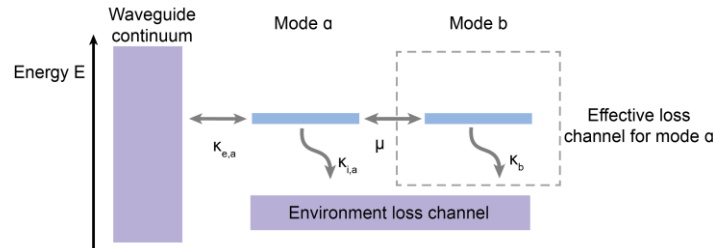
We have transitioned to the laser rotating frame $a \rightarrow ae^{i\omega_L t}$, $b \rightarrow be^{i\omega_L t}$ with $\Delta_a = \omega_L - \omega_a$ and $\Delta_b = \omega_L - \omega_b$ (ω_L , ω_a , ω_b are the frequency of laser, a , and b , respectively). Steady state solution ($\dot{a}, \dot{b} = 0$) gives an effective equation for a

$$0 = \left[-i(\Delta_a + \Delta_{eff}) - \frac{(\kappa_{e,a} + \kappa_{i,a} + \kappa_{eff})}{2}\right]a - \sqrt{\kappa_{e,a}}a_{in}$$

In which

$$\Delta_{eff} = -\Delta_b \frac{\mu^2}{\frac{\kappa_b^2}{4} + \Delta_b^2} \quad \kappa_{eff} = \kappa_b \frac{\mu^2}{\frac{\kappa_b^2}{4} + \Delta_b^2}$$

Therefore, coupling to a resonant mode b introduces an effective detuning and loss rate for mode a . The GCC can be achieved when $\kappa_{e,a} = \kappa_{i,a} + \kappa_{eff}$ and $\Delta_a + \Delta_{eff} = 0$. By manipulating the loss rates under GCC, energy flow can be engineered. For instance, when $\kappa_{e,a} \sim \kappa_{eff} \gg \kappa_{i,a}$, nearly 100% of the energy is directed towards mode b , thus preventing wastage of energy through channel $\kappa_{i,a}$.



Box Figure 2 | Illustration of the general critical coupling.

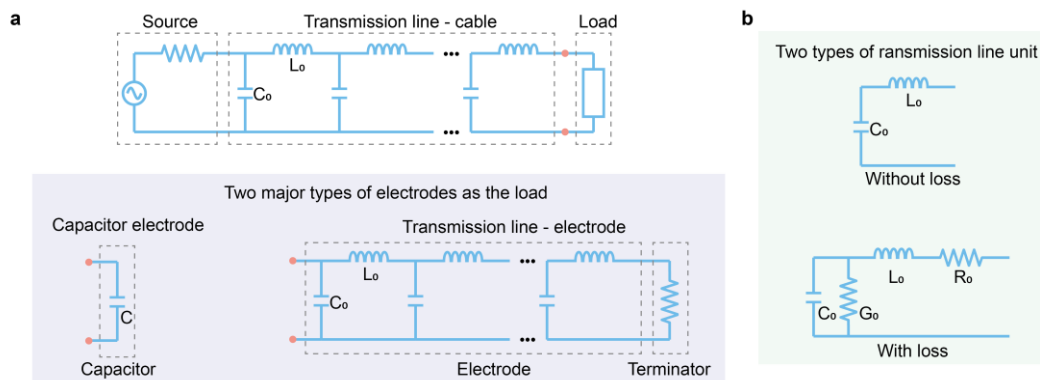
In many cases, it is common to simplify the system by setting $\Delta_a = \Delta_b = 0$. In this case, the physical picture is: a resonance-coupling induces a loss channel equivalent to $\kappa_{eff} = 4\mu^2/\kappa_b$, with μ is the resonant coupling and κ_b is the mode that causes this loss. This simplification aids in a quick estimation of the loss induced by resonance-coupling. Note that this also applies to multiple levels coupled as a chain. The effective loss created by a chain of levels can be obtained by cascading this equivalent loss calculation (e.g. the process of cavity EO comb generation⁶). The GCC can be a useful tool for manipulating energy flow in systems with multiple resonant modes, such as coupled-cavity system as well as applications in frequency shifting³, EO comb⁶, Kerr comb^{225,226}, nonlinear frequency conversion²²⁷, and more.

Box 3 Microwave engineering for EO modulation

The bandwidth of an EO modulator critically relies on the microwave engineering of its electrode. Here we discuss some basic concepts of microwave engineering. The electrode is typically classified as lumped element or distributed element, determined by the electrode characteristic size L and the wavelength of the microwave. For example, when the wavelength λ_{MW} of the applied microwave is much larger than the electrode size L , the electrode can be treated as a pure capacitor with resistance and inductance. When $\lambda_{MW} \sim L$ or $\lambda_{MW} \ll L$, distributed models should be used.

In the simple case where the electrode is a capacitor, the modulator's frequency response is limited by the RC (resistance-capacitance) time-constant of the electrode. Long electrodes with narrow gaps can enhance interaction and reduce V_{π} , but they also increase capacitance, resulting in smaller bandwidth. To overcome this limit, traveling-wave modulators are required, where the electrode is designed to be a transmission line (distributed element), allowing microwave to co-propagate with the optical field at the same speed. In this case, velocity matching (microwave phase velocity matching optical group velocity), impedance matching, and microwave loss are important considerations. A detailed discussion of traveling-wave modulator design can be found in Section 3.2 of Ref ⁴⁵. Different from bulk LN modulator, where the dielectric environment of the transmission line is almost fixed, the microwave velocity (i.e., microwave index) in TFLN modulators can be effectively engineered by adjusting the thickness of buried and cladding oxide and achieve nearly perfect velocity matching.

To understand the microwave behavior of a practical EO modulator system, it is helpful to describe the RF source, cable, and modulator electrode in the form of a distributed circuit model (see Box Figure below). The RF cable and transmission line electrodes can both be modeled using LC ladders, and the characteristic impedance is $\sqrt{L/C}$, where L and C are inductance and capacitance per unit length. Note that the source has an output impedance, R_{source} , commonly at 50 Ohm. When measuring low-frequency response of capacitive load or unterminated transmission line (a common configuration for V_{π} measurement), the actual voltage on the device can be twice as the voltage displayed on the waveform/signal generator, since the displayed values are rated to matched load. This is a common mistake that can lead to underestimation of modulator V_{π} in experimental measurement.



Box Figure 3 | a, Basic concept of microwave engineering for efficient modulation on TFLN. The transmission line impedance is given by $Z_0 = \sqrt{L_0/C_0}$. **b**, Illustration of transmission line unit cell with and without losses. In a), unit cells without loss are used as an example. The resistance R_0 and conductance G_0 contribute to the microwave propagation loss in the transmission line.

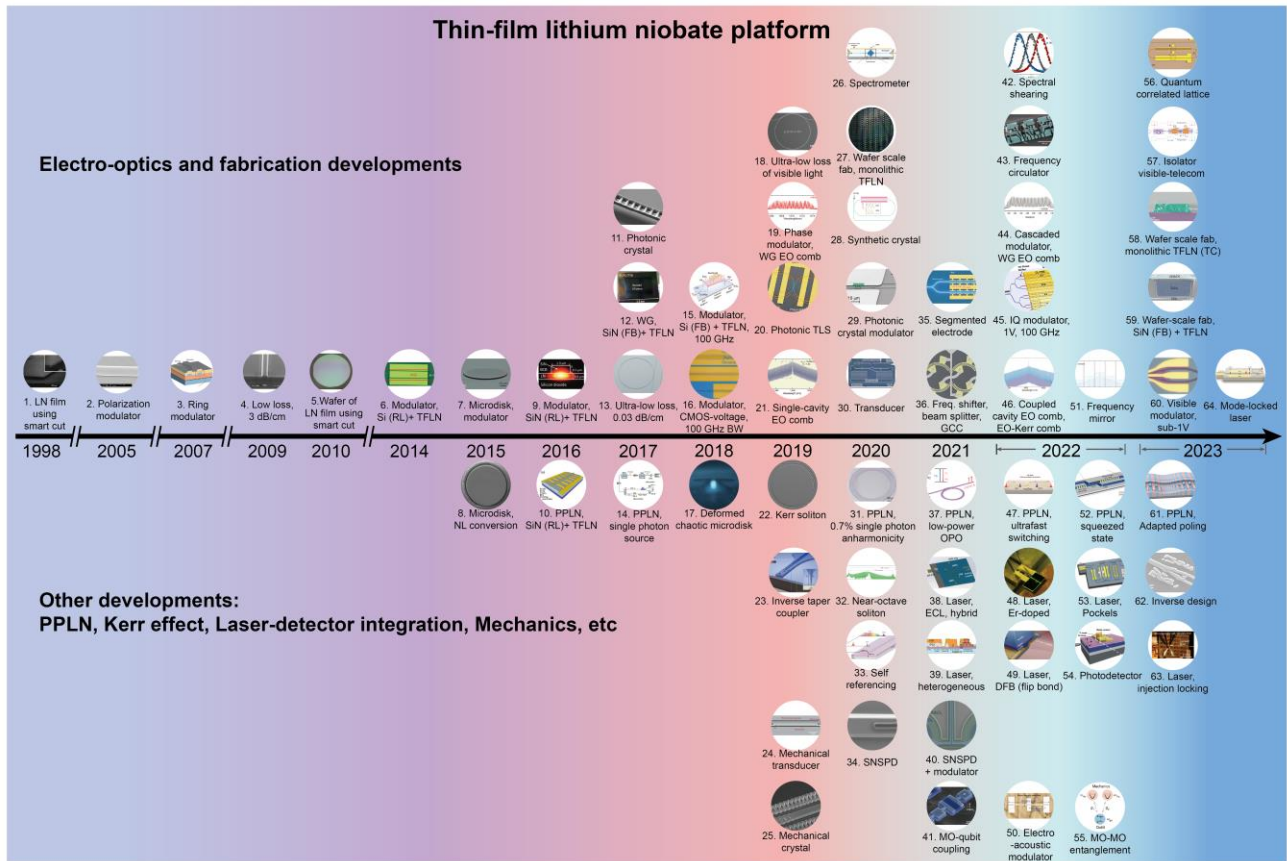


Fig. 1 | Time-line of various thin-film lithium niobate platforms development. Upper panel shows the development of TFLN electro-optics, while the bottom one shows the development of related TFLN platforms including periodically-poled TFLN (PP-TFLN), III-V-TFLN integration, etc. Type of integration is indicated for heterogeneous/hybrid integrated platforms, while those without the label are monolithic TFLN. **Abbreviations:** RL, rib-loaded; FB, film-bonding; NL, nonlinear; PPLN, periodically-poled lithium niobate; WG, waveguide; TLS, two-level-system; GCC, general critical coupling; MO, mechanical oscillator; SNSPD, superconducting nanowire single photon detector; OPO, optical parametric oscillation; ECL, external cavity laser; TC, tight-confining; DFB, distributed feedback; CMOS, complementary metal-oxide semiconductor; LN, lithium niobate; TFLN, thin-film lithium niobate; Si, silicon; SiN, silicon nitride; **References:** 1. LN film using smart cut: ref. ⁴⁰, together with others²²⁸; 2. Polarization modulator: ref. ²²⁹; 3. Ring modulator: ref. ⁹⁵; 4. Low loss, 3 dB/cm: ref. ⁴¹; 5. Wafer of LN film using smart cut: ref. ²³⁰; 6. Modulator, Si (RL) + TFLN: ref. ⁶⁶, together with others^{67–69}; 7. Microdisk, modulator: ref. ²³¹, together with others^{232–235}; 8. Microdisk, NL conversion: ref. ²³⁶, together with others^{237–245}; 9. Modulator, SiN (RL) + TFLN: ref. ⁷², together with others^{70,71,73–75}; 10. PPLN, SiN (RL) + TFLN: ref. ⁷⁶; 11. Photonic crystal: ref. ²⁴⁶, together with others^{99,247–250}; 12. WG, SiN (FB) + TFLN: ref. ⁶², together with others⁶³; 13. Ultra-low loss, 0.03 dB/cm: ref. ⁴³; 14. PPLN, single photon source: ref. ²⁵¹, together with others²⁵²; 15. Modulator, Si (FB) + TFLN 100 GHz: ref. ⁶⁰, together with others⁶¹; 16. Modulator, CMOS-voltage, 100 GHz BW: ref. ¹; 17. Deformed chaotic microdisk: ref. ²⁵³; 18. Ultra-low loss of visible light: ref. ⁴⁴; 19. Phase modulator, WG EO comb: ref. ⁴⁸; 20. Photonic TLS: ref. ⁸; 21. Single cavity EO comb: ref. ², together with others¹²³; 22. Kerr soliton: ref. ¹⁶⁷, together with others¹⁶⁶; 23. Inverse taper coupler: ref. ²⁵⁴; 24. Mechanical transducer: ref. ²⁵⁵, together with others²⁴⁹; 25. Mechanical crystal: ref. ²⁴⁸; 26. Spectrometer: ref. ²⁵⁶; 27. Wafer scale fab, monolithic TFLN: ref. ²⁵⁷; 28. Synthetic crystal: ref. ¹⁴; 29. Photonic crystal modulator: ref. ⁹⁸; 30. Transducer: ref. ¹⁹, together with others^{18,20}; 31. PPLN, 0.7% single photon anharmonicity: ref. ¹⁷⁶; 32. Near-octave soliton: ref. ¹⁶⁸; 33. Self referencing: ref. ²⁵⁸; 34. SNSPD: ref. ²⁵⁹, together with others²⁶⁰; 35. Segmented electrode: ref. ⁵², together with others^{82–84}; 36.

Freq. shifter, beam splitter, GCC: ref. ³; 37. PPLN low-power OPO: ref. ²⁶¹, together with others²⁶²; 38 Laser, ECL, hybrid: ref. ¹⁵⁷; 39. Laser, heterogeneous: ref. ¹⁶³, together with others^{162,164,165}; 40. SNSPD + modulator: ref. ²⁶³; 41. MO-qubit coupling: ref. ²⁶⁴; 42. Frequency circulator: ref. ⁷; 43. Spectral shearing: ref. ¹²; 44. Cascaded modulator, WG EO comb: ref. ⁹, together with others¹¹¹; 45. IQ modulator: ref. ⁵, together with others^{85,86}; 46. Coupled cavity EO comb, EO-Kerr comb: ref. ⁶; 47. PPLN, ultrafast switching: ref. ²⁶⁵; 48. Laser, Er-doped: ref. ¹⁵⁶, together with others¹⁵⁵; 49. Laser, DFB (flip bond): ref. ¹⁶⁰; 50. Electro-acoustic modulator: ref. ¹⁹⁵; 51. Frequency mirror: ref. ¹³; 52. PPLN, squeezed state: ref. ¹⁹³; 53. Laser, Pockels: ref. ¹⁵⁹; 54. Photodetector: ref. ¹⁶⁹, together with others^{164,170}; 55. MO-MO entanglement: ref. ²⁶⁶; 56. Quantum correlated lattice: ref. ¹⁵; 57. Visible-telecom isolator: ref. ²⁶⁷, together with others²⁶⁸; 58. Wafer scale fab, monolithic (TC): ref. ²⁶⁹; 59. Wafer scale fab, SiN (FB) + TFLN: ref. ⁶⁴, together with others^{65,158}; 60. Visible modulator, sub-1V: ref. ¹¹, together with others¹⁰; 61. PPLN, adapted poling: ref. ²⁷⁰; 62. Inverse design: ref. ²⁷¹; 63. Laser, injection locking: ref. ¹⁵⁸; 64. Mode-locked laser: ref. ²²⁰;

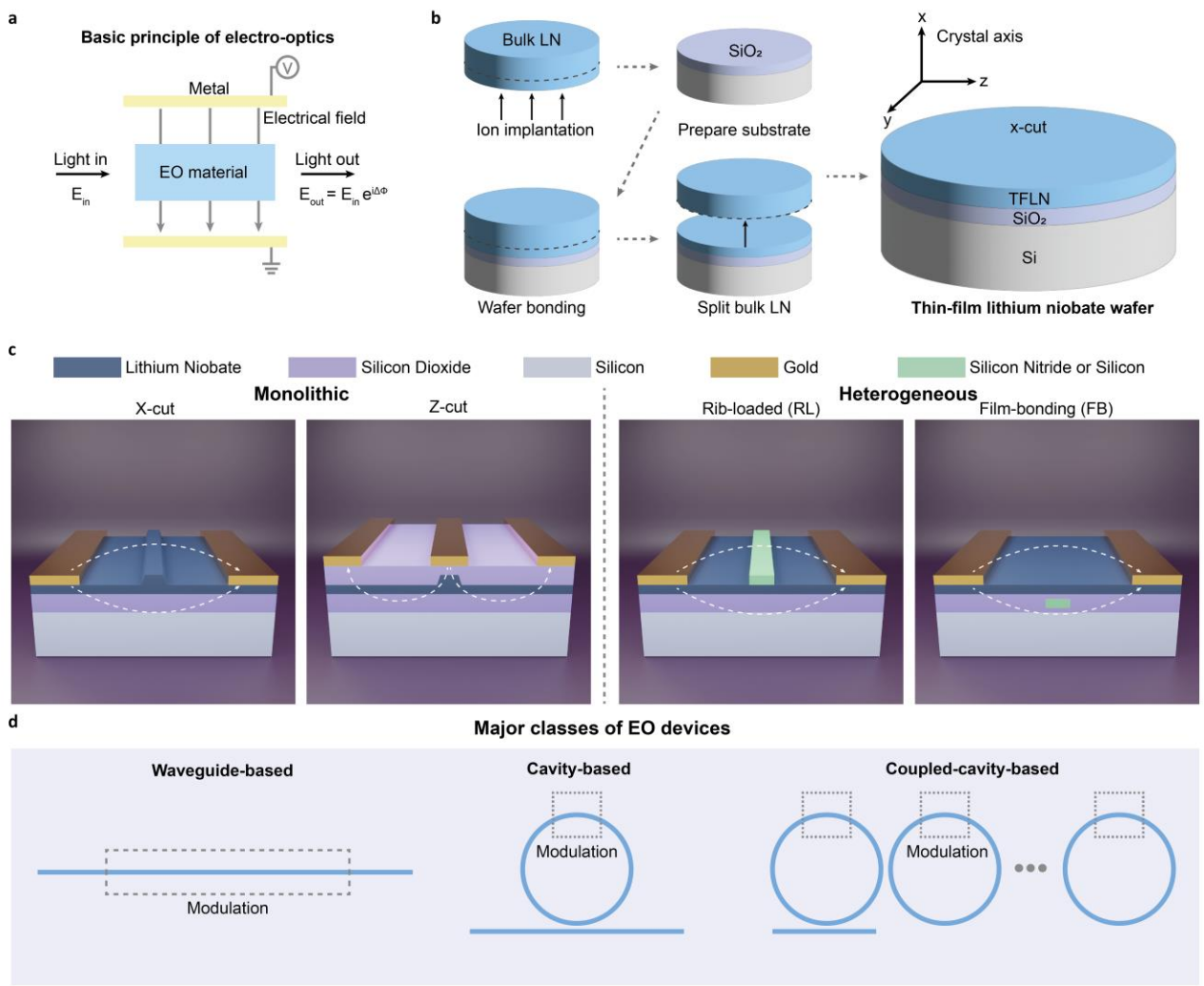


Fig. 2 | Basic principle and device structures on thin-film lithium niobate. **a**, Light sent into an EO material will acquire a phase shift that is proportional to the voltage applied to the material. **b**, Illustration of TFLN wafer and the “smart cut” technology used to prepare the TFLN wafer. The axis represents the crystal axis of the LN crystal. **c**, Cross-section for major types of TFLN EO platforms. The white dashed arrows denote the microwave electric field line. **d**, Illustration of three major classes of EO devices: waveguide, cavity, and coupled-cavity. The dashed box is used to label the electrode region for applying EO modulation.

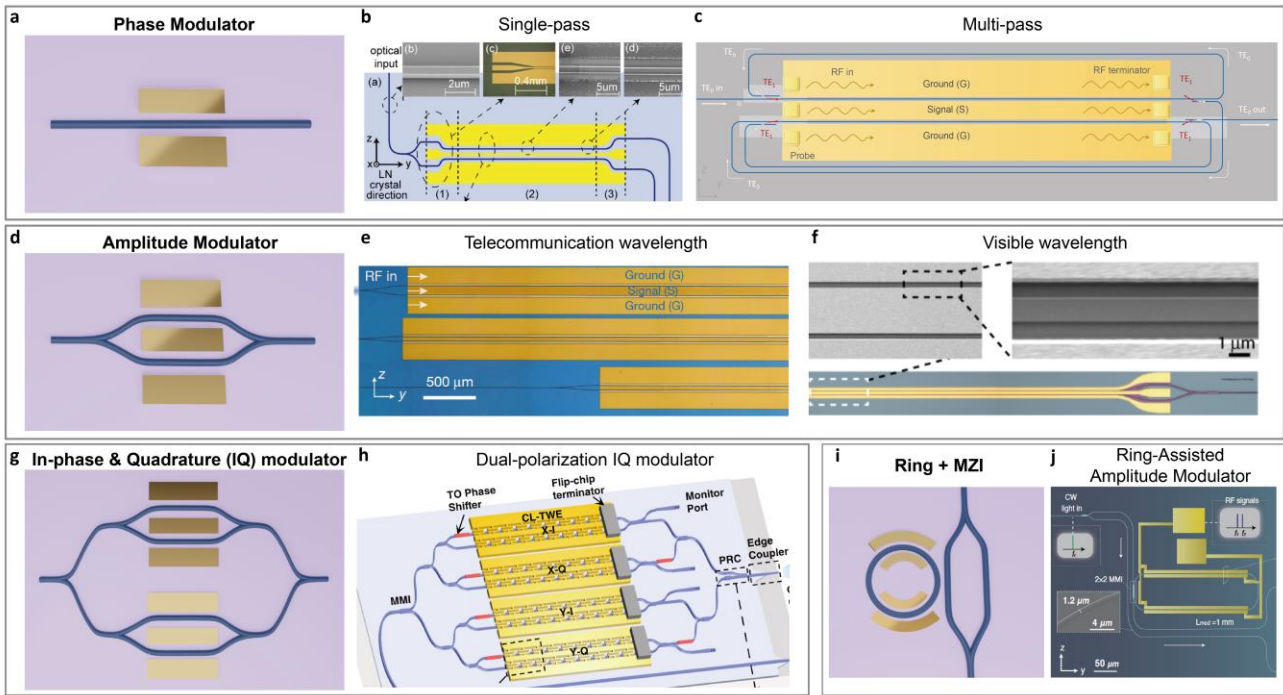


Fig. 3 | Waveguide-based devices on thin-film lithium niobate. **a**, Schematic configuration of PM. It contains a single waveguide with electrode. Voltage changes the phase of the light. **b**, Representative device image of a conventional TFLN PM. Input light is split into two paths. Light transmitted through the electrode region obtains a phase modulation. Two output ports are designed to receive light from each path. **c**, Representative device image of multi-pass PM. Light can transmit through the phase modulation region four-times through TE₀/TE₁ mode conversion. **d**, Schematic configuration of AM. Light is split into two paths with reversed-sign phase modulation. Interference occurs after passing through the electrode via the output splitter, converting the phase modulation to an amplitude modulation. **e**, Representative device image of AM with CMOS-compatible voltage and 100 GHz EO bandwidth at telecommunication wavelength. **f**, Representative device image of an AM at visible wavelength, featuring a $V_{\pi} \cdot L$ as low as 0.17 V · cm at 400nm. **g**, Schematic configuration of an IQ modulator. Two amplitude modulators form an interferometer, with each paths having a $\frac{\pi}{2}$ relative phase delay on microwave drive signal, allowing modulation in the complex space of in-phase and quadrature components. **h**, Representative device image of a dual-polarization IQ modulator, in which two IQ modulators with different polarizations are used in parallel and combined in the end, allowing polarization multiplexing. **i**, Schematic configuration of a ring-assisted AM. **j**, Representative device image of a ring-assisted AM for improving the linearity of an AM. Panels adapted with permission from: **b**, ref ⁴⁸, IEEE; **c**, ref ⁹¹, Springer Nature Ltd; **e**, ref ¹, Springer Nature Ltd; **f**, ref ¹¹, Optica; **h**, ref ⁵, Optica; **j**, ref ⁹⁰, Springer Nature Ltd;

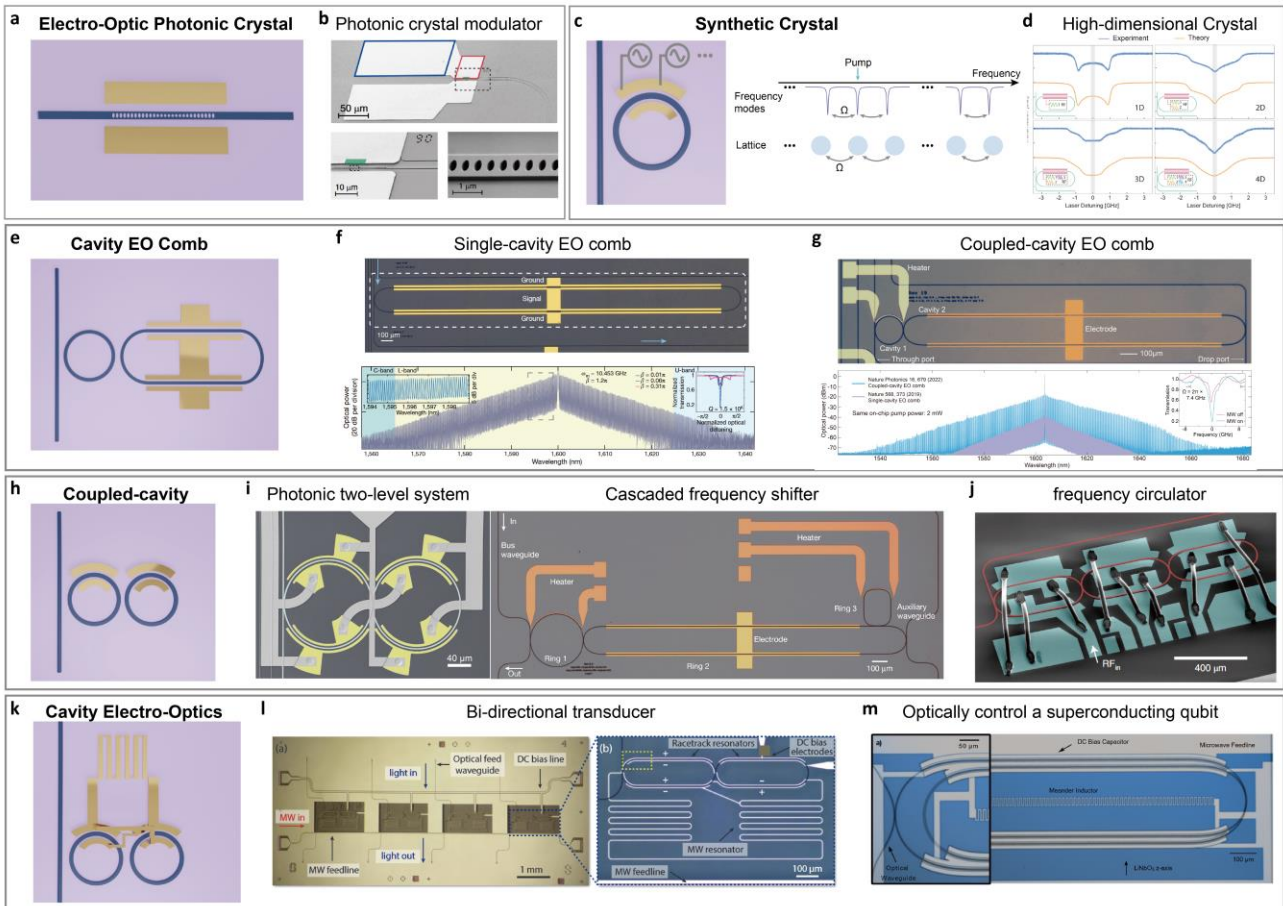


Fig. 4 | Cavity-based EO devices on thin-film lithium niobate. **a**, Schematic configuration of a photonic crystal modulator. **b**, Representative device image of photonic crystal modulator. **c**, Schematic of a synthetic EO crystal. **d**, Representative data of a high-dimensional frequency crystal. **e**, schematic configuration of a coupled-cavity EO comb. **f**, representative device image of a single cavity EO comb; **g**, representative device image of a coupled-cavity EO comb; **h**, schematic configuration of a double-ring coupled-cavity EO modulator. Two identical rings form a photonic TLS. Microwave modulation drives the transition. **i**, representative device image of a photonic TLS as well as a frequency shifter and beam splitter. In a cascaded frequency shifter, light flows through a ladder of energy levels. This allows one to shift the light frequency beyond 100 GHz using only a continuous and single-tone microwave at several tens of GHz. **j**, Representative device image of a triple-ring coupled-cavity frequency circulator, enabling 40 dB isolation with only 75 mW microwave power. **k**, Schematic configuration of a cavity electro-optics device, formed by a lumped-element microwave cavity coupled to an optical cavity. **l**, **m**, representative device image for cavity electro-optics, including transducers and optical control of a superconducting qubit. Panels adapted with permission from: **b**, ref. ⁹⁸, Springer Nature Ltd; **d**, ref. ¹⁴, Optica; **f**, ref. ² Springer Nature Ltd; **g**, ref. ⁶, Springer Nature Ltd; **i**, ref ³, Springer Nature Ltd; **j**, ref. ⁷, Springer Nature Ltd; **l**, ref. ¹⁹, Optica; **m**, ref. ¹⁴⁵, arXiv;

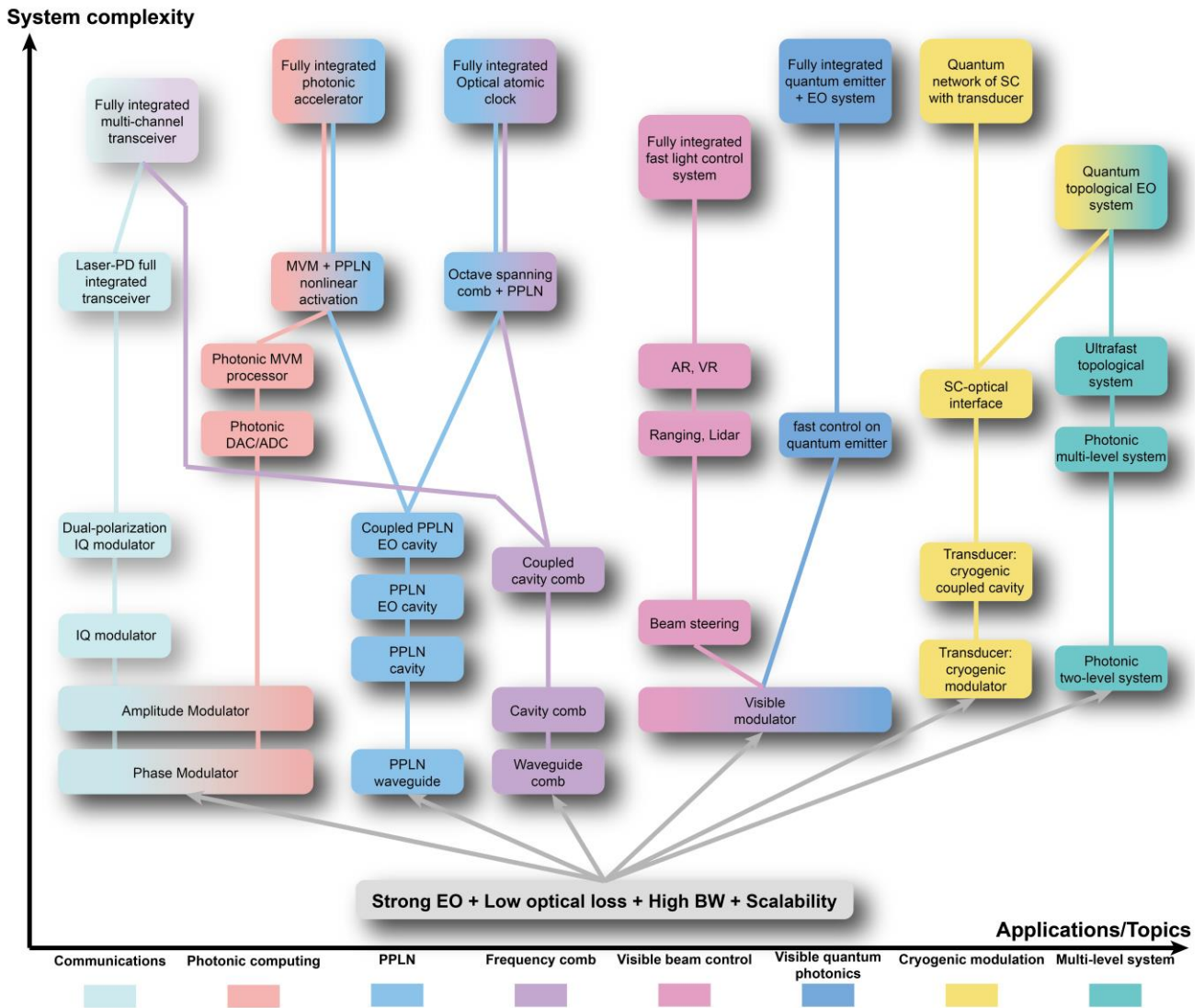


Fig. 5 | Evolution and outlook for applications of integrated EO system on thin-film lithium niobate. The height of the tree denotes the system complexity while each branch of the tree represents one topic or application. Some of the branches merge as the complexity increases, leading to more advanced systems. Abbreviation in the figure: MVM, matrix-vector multiplication; DAC, digital-to-analog converter; ADC, analog-to-digital converter; PD, photodiode; PPLN, periodically poled lithium niobate; IQ, in-phase and quadrature; AM, amplitude modulator; PM, phase modulator; EO, electro-optics; AR, augmented reality; VR, virtual reality; SC, superconducting qubit.

References

1. Wang, C. *et al.* Integrated lithium niobate electro-optic modulators operating at CMOS-compatible voltages. *Nature* **562**, 101–104 (2018).
2. Zhang, M. *et al.* Broadband electro-optic frequency comb generation in a lithium niobate microring resonator. *Nature* **568**, 373–377 (2019).
3. Hu, Y. *et al.* On-chip electro-optic frequency shifters and beam splitters. *Nature* **599**, 587–593 (2021).
4. He, M. *et al.* High-performance hybrid silicon and lithium niobate Mach–Zehnder modulators for 100 Gbit s⁻¹ and beyond. *Nat. Photonics* **13**, 359–364 (2019).
5. Xu, M. *et al.* Dual-polarization thin-film lithium niobate in-phase quadrature modulators for terabit-per-second transmission. *Optica* **9**, 61 (2022).
6. Hu, Y. *et al.* High-efficiency and broadband on-chip electro-optic frequency comb generators. *Nat. Photonics* **16**, 679–685 (2022).
7. Herrmann, J. F. *et al.* Mirror symmetric on-chip frequency circulation of light. *Nat. Photonics* **16**, 603–608 (2022).
8. Zhang, M. *et al.* Electronically programmable photonic molecule. *Nat. Photonics* **13**, 36–40 (2019).
9. Yu, M. *et al.* Integrated femtosecond pulse generator on thin-film lithium niobate. *Nature* **612**, 252–258 (2022).
10. Renaud, D. *et al.* Sub-1 Volt and high-bandwidth visible to near-infrared electro-optic modulators. *Nat. Commun.* **14**, 1496 (2023).
11. Xue, S. *et al.* Full-spectrum visible electro-optic modulator. *Optica* **10**, 125 (2023).
12. Zhu, D. *et al.* Spectral control of nonclassical light pulses using an integrated thin-film lithium niobate modulator. *Light Sci. Appl.* **11**, 327 (2022).
13. Hu, Y. *et al.* Mirror-induced reflection in the frequency domain. *Nat. Commun.* **13**, 6293 (2022).
14. Hu, Y. *et al.* Realization of high-dimensional frequency crystals in electro-optic microcombs. *Optica* **7**, 1189–1194 (2020).
15. Javid, U. A. *et al.* Chip-scale simulations in a quantum-correlated synthetic space. *Nat. Photonics* (2023) doi:10.1038/s41566-023-01236-7.
16. Wang, J. *et al.* Topologically tuned terahertz confinement in a nonlinear photonic chip. *Light Sci. Appl.* **11**, 152 (2022).
17. Gorbach, A. V., Beer, J. & Souslov, A. Topological edge states in equidistant arrays of Lithium Niobate nano-waveguides. Preprint at <http://arxiv.org/abs/2303.00809> (2023).
18. Holzgrafe, J. *et al.* Cavity electro-optics in thin-film lithium niobate for efficient microwave-to-optical transduction. *Optica* **7**, 1714–1720 (2020).

19. McKenna, T. P. *et al.* Cryogenic microwave-to-optical conversion using a triply resonant lithium-niobate-on-sapphire transducer. *Optica* **7**, 1737–1745 (2020).
20. Xu, Y. *et al.* Bidirectional interconversion of microwave and light with thin-film lithium niobate. *Nat. Commun.* **12**, 4453 (2021).
21. Yoo, S. J. B. Wavelength conversion technologies for WDM network applications. *J. Light. Technol.* **14**, 955–966 (1996).
22. Nakajima, K., Matsui, T., Saito, K., Sakamoto, T. & Araki, N. Multi-Core Fiber Technology: Next Generation Optical Communication Strategy. *IEEE Commun. Stand. Mag.* **1**, 38–45 (2017).
23. Kaushal, H. & Kaddoum, G. Optical Communication in Space: Challenges and Mitigation Techniques. *IEEE Commun. Surv. Tutor.* **19**, 57–96 (2017).
24. Mukherjee, B. WDM optical communication networks: progress and challenges. *IEEE J. Sel. Areas Commun.* **18**, 1810–1824 (2000).
25. Kikuchi, K. Fundamentals of Coherent Optical Fiber Communications. *J. Light. Technol.* **34**, 157–179 (2016).
26. Riemensberger, J. *et al.* Massively parallel coherent laser ranging using a soliton microcomb. *Nature* **581**, 164–170 (2020).
27. Zhang, X., Kwon, K., Henriksson, J., Luo, J. & Wu, M. C. A large-scale microelectromechanical-systems-based silicon photonics LiDAR. *Nature* **603**, 253–258 (2022).
28. Fujimoto, J. G. Optical coherence tomography for ultrahigh resolution in vivo imaging. *Nat. Biotechnol.* **21**, 1361–1367 (2003).
29. Siddiqui, M. *et al.* High-speed optical coherence tomography by circular interferometric ranging. *Nat. Photonics* **12**, 111–116 (2018).
30. Wetzstein, G. *et al.* Inference in artificial intelligence with deep optics and photonics. *Nature* **588**, 39–47 (2020).
31. Shastri, B. J. *et al.* Photonics for artificial intelligence and neuromorphic computing. *Nat. Photonics* **15**, 102–114 (2021).
32. Nahmias, M. A. *et al.* Photonic Multiply-Accumulate Operations for Neural Networks. *IEEE J. Sel. Top. Quantum Electron.* **26**, 1–18 (2020).
33. Berggren, K. *et al.* Roadmap on emerging hardware and technology for machine learning. *Nanotechnology* **32**, 012002 (2021).
34. McMahon, P. L. The physics of optical computing. *Nat. Rev. Phys.* **5**, 717–734 (2023).
35. Marpaung, D., Yao, J. & Capmany, J. Integrated microwave photonics. *Nat. Photonics* **13**, 80–90 (2019).

36. Seeds, A. J. & Williams, K. J. Microwave Photonics. *J. Light. Technol.* **24**, 4628–4641 (2006).
37. Yao, J. Microwave Photonics. *J. Light. Technol.* **27**, 314–335 (2009).
38. Capmany, J. & Novak, D. Microwave photonics combines two worlds. *Nat. Photonics* **1**, 319–330 (2007).
39. Eggleton, B. J., Poulton, C. G., Rakich, P. T., Steel, Michael. J. & Bahl, G. Brillouin integrated photonics. *Nat. Photonics* **13**, 664–677 (2019).
40. Levy, M. *et al.* Fabrication of single-crystal lithium niobate films by crystal ion slicing. *Appl. Phys. Lett.* **73**, 2293–2295 (1998).
41. Hu, H., Ricken, R. & Sohler, W. Large area, crystal-bonded LiNbO₃ thin films and ridge waveguides of high refractive index contrast. in (2009).
42. Hu, H., Gui, L., Ricken, R. & Sohler, W. Towards nonlinear photonic wires in lithium niobate. in (eds. Broquin, J.-E. & Greiner, C. M.) 76040R (San Francisco, California, 2010). doi:10.1117/12.842674.
43. Zhang, M., Wang, C., Cheng, R., Shams-Ansari, A. & Lončar, M. Monolithic ultra-high-Q lithium niobate microring resonator. *Optica* **4**, 1536 (2017).
44. Desiatov, B., Shams-Ansari, A., Zhang, M., Wang, C. & Lončar, M. Ultra-low-loss integrated visible photonics using thin-film lithium niobate. *Optica* **6**, 380 (2019).
45. Zhu, D. *et al.* Integrated photonics on thin-film lithium niobate. *Adv. Opt. Photonics* **13**, 242 (2021).
46. Boes, A. *et al.* Lithium niobate photonics: Unlocking the electromagnetic spectrum. *Science* **379**, eabj4396 (2023).
47. Chen, G. *et al.* Advances in lithium niobate photonics: development status and perspectives. *Adv. Photonics* **4**, (2022).
48. Ren, T. *et al.* An Integrated Low-Voltage Broadband Lithium Niobate Phase Modulator. *IEEE Photonics Technol. Lett.* **31**, 889–892 (2019).
49. Örsel, O. E. & Bahl, G. Electro-optic non-reciprocal polarization rotation in lithium niobate. *APL Photonics* **8**, 096107 (2023).
50. Reimer, C. *et al.* Generation of multiphoton entangled quantum states by means of integrated frequency combs. *Science* **351**, 1176–1180 (2016).
51. Yu, Z. & Fan, S. Complete optical isolation created by indirect interband photonic transitions. *Nat. Photonics* **3**, 91–94 (2009).
52. Kharel, P., Reimer, C., Luke, K., He, L. & Zhang, M. Breaking voltage–bandwidth limits in integrated lithium niobate modulators using micro-structured electrodes. *Optica* **8**, 357 (2021).

53. Vazimali, M. G. & Fathpour, S. Applications of thin-film lithium niobate in nonlinear integrated photonics. *Adv. Photonics* **4**, (2022).
54. Sinatkas, G., Christopoulos, T., Tsilipakos, O. & Kriezis, E. E. Electro-optic modulation in integrated photonics. *J. Appl. Phys.* **130**, 010901 (2021).
55. Zhang, M., Wang, C., Kharel, P., Zhu, D. & Lončar, M. Integrated lithium niobate electro-optic modulators: when performance meets scalability. *Optica* **8**, 652 (2021).
56. Chen, G., Gao, Y., Lin, H.-L. & Danner, A. J. Compact and Efficient Thin-Film Lithium Niobate Modulators. (2023).
57. Boyd, R. W. *Nonlinear Optics*. (Elsevier, 2008).
58. Haus, H. A. *Waves and Fields in Optoelectronics*. (Prentice-Hall, 1984).
59. Yariv, A. & Yeh, P. *Photonics: Optical Electronics in Modern Communications*. (Oxford University Press, 2007).
60. Weigel, P. O. *et al.* Bonded thin film lithium niobate modulator on a silicon photonics platform exceeding 100 GHz 3-dB electrical modulation bandwidth. *Opt. Express* **26**, 23728 (2018).
61. He, M. *et al.* High-performance hybrid silicon and lithium niobate Mach–Zehnder modulators for 100 Gbit s⁻¹ and beyond. *Nat. Photonics* **13**, 359–364 (2019).
62. Chang, L. *et al.* Heterogeneous integration of lithium niobate and silicon nitride waveguides for wafer-scale photonic integrated circuits on silicon. *Opt. Lett.* **42**, 803 (2017).
63. Vanackere, T. *et al.* Heterogeneous integration of a high-speed lithium niobate modulator on silicon nitride using micro-transfer printing. *APL Photonics* **8**, 086102 (2023).
64. Churaev, M. *et al.* A heterogeneously integrated lithium niobate-on-silicon nitride photonic platform. *Nat. Commun.* **14**, 3499 (2023).
65. Ghosh, S. *et al.* Wafer-scale heterogeneous integration of thin film lithium niobate on silicon-nitride photonic integrated circuits with low loss bonding interfaces. *Opt. Express* **31**, 12005 (2023).
66. Cao, L., Aboketaf, A., Wang, Z. & Preble, S. Hybrid amorphous silicon (a-Si:H)–LiNbO₃ electro-optic modulator. *Opt. Commun.* **330**, 40–44 (2014).
67. Wang, Y. *et al.* Amorphous silicon-lithium niobate thin film strip-loaded waveguides. *Opt. Mater. Express* **7**, 4018–4028 (2017).
68. Zhu, H. *et al.* Hybrid mono-crystalline silicon and lithium niobate thin films [Invited]. *Chin. Opt. Lett.* **19**, 060017 (2021).

69. Li, Q., Zhu, H., Zhang, H., Cai, L. & Hu, H. Phase modulators in hybrid silicon and lithium niobate thin films. *Opt. Mater. Express* **12**, 1314 (2022).
70. Chang, L. *et al.* Thin film wavelength converters for photonic integrated circuits. *Optica* **3**, 531 (2016).
71. Jin, S., Xu, L., Zhang, H. & Li, Y. LiNbO₃ Thin-Film Modulators Using Silicon Nitride Surface Ridge Waveguides. *IEEE Photonics Technol. Lett.* **28**, 736–739 (2016).
72. Rao, A. *et al.* High-performance and linear thin-film lithium niobate Mach–Zehnder modulators on silicon up to 50 GHz. *Opt. Lett.* **41**, 5700 (2016).
73. Mehta, K. K., West, G. N. & Ram, R. J. SiN-on-LiNbO₃ integrated optical modulation at visible wavelengths. in *2017 Conference on Lasers and Electro-Optics (CLEO) 1–2* (2017).
74. Rao, A. & Fathpour, S. Heterogeneous Thin-Film Lithium Niobate Integrated Photonics for Electrooptics and Nonlinear Optics. *IEEE J. Sel. Top. Quantum Electron.* **24**, 1–12 (2018).
75. Ahmed, A. N. R., Shi, S., Zablocki, M., Yao, P. & Prather, D. W. Tunable hybrid silicon nitride and thin-film lithium niobate electro-optic microresonator. *Opt. Lett.* **44**, 618–621 (2019).
76. Rao, A. *et al.* Second-harmonic generation in periodically-poled thin film lithium niobate wafer-bonded on silicon. *Opt. Express* **24**, 29941 (2016).
77. Sun, S. *et al.* Bias-drift-free Mach–Zehnder modulators based on a heterogeneous silicon and lithium niobate platform. *Photonics Res.* **8**, 1958 (2020).
78. Wang, Z. *et al.* Silicon–Lithium Niobate Hybrid Intensity and Coherent Modulators Using a Periodic Capacitively Loaded Traveling-Wave Electrode. *ACS Photonics* **9**, 2668–2675 (2022).
79. Mookherjea, S., Mere, V. & Valdez, F. Thin-film lithium niobate electro-optic modulators: To etch or not to etch. *Appl. Phys. Lett.* **122**, 120501 (2023).
80. Mercante, A. J. *et al.* 110 GHz CMOS compatible thin film LiNbO₃ modulator on silicon. *Opt. Express* **24**, 15590 (2016).
81. Mercante, A. J. *et al.* Thin film lithium niobate electro-optic modulator with terahertz operating bandwidth. *Opt. Express* **26**, 14810 (2018).
82. Chen, G. *et al.* High performance thin-film lithium niobate modulator on a silicon substrate using periodic capacitively loaded traveling-wave electrode. *APL Photonics* **7**, 026103 (2022).
83. Nelan, S. P. *et al.* Integrated Lithium Niobate Intensity Modulator on a Silicon Handle With Slow-Wave Electrodes. *IEEE Photonics Technol. Lett.* **34**, 981–984 (2022).

84. Valdez, F. *et al.* 110 GHz, 110 mW hybrid silicon-lithium niobate Mach-Zehnder modulator. *Sci. Rep.* **12**, 18611 (2022).
85. Xu, M. *et al.* High-performance coherent optical modulators based on thin-film lithium niobate platform. *Nat. Commun.* **11**, 3911 (2020).
86. Wang, X. *et al.* Thin-film lithium niobate dual-polarization IQ modulator on a silicon substrate for single-carrier 1.6 Tb/s transmission. *APL Photonics* **7**, 076101 (2022).
87. Xu, M. *et al.* Attojoule/bit folded thin film lithium niobate coherent modulators using air-bridge structures. *APL Photonics* **8**, 066104 (2023).
88. Liu, X. *et al.* Broadband Meandered Thin-Film Lithium Niobate Modulator With Ultra-Low Half-Wave Voltage. *IEEE Photonics Technol. Lett.* **34**, 424–427 (2022).
89. Zhang, Y. *et al.* Systematic investigation of millimeter-wave optic modulation performance in thin-film lithium niobate. *Photonics Res.* **10**, 2380 (2022).
90. Feng, H. *et al.* Ultra-high-linearity integrated lithium niobate electro-optic modulators. *Photonics Res.* **10**, 2366 (2022).
91. Zhang, K. *et al.* A power-efficient integrated lithium niobate electro-optic comb generator. *Commun. Phys.* **6**, 17 (2023).
92. Pohl, D. *et al.* High-Bandwidth Lithium Niobate Electro-Optic Modulator at Visible-Near-Infrared Wavelengths. in *European Conference on Optical Communication (ECOC) 2022 (2022)*, paper Tu4E.1 Tu4E.1 (Optica Publishing Group, 2022).
93. Sund, P. I. *et al.* High-speed thin-film lithium niobate quantum processor driven by a solid-state quantum emitter. *Sci. Adv.* **9**, eadg7268 (2023).
94. Christen, I. *et al.* An integrated photonic engine for programmable atomic control. Preprint at <http://arxiv.org/abs/2208.06732> (2022).
95. Guarino, A., Poberaj, G., Rezzonico, D., Degl’Innocenti, R. & Günter, P. Electro–optically tunable microring resonators in lithium niobate. *Nat. Photonics* **1**, 407–410 (2007).
96. Wang, C., Zhang, M., Stern, B., Lipson, M. & Lončar, M. Nanophotonic lithium niobate electro-optic modulators. *Opt. Express* **26**, 1547 (2018).
97. Bahadori, M., Yang, Y., Hassanien, A. E., Goddard, L. L. & Gong, S. Ultra-efficient and fully isotropic monolithic microring modulators in a thin-film lithium niobate photonics platform. *Opt. Express* **28**, 29644 (2020).
98. Li, M. *et al.* Lithium niobate photonic-crystal electro-optic modulator. *Nat. Commun.* **11**, 4123 (2020).

99. Witmer, J. D. *et al.* High-Q photonic resonators and electro-optic coupling using silicon-on-lithium-niobate. *Sci. Rep.* **7**, 46313 (2017).
100. Xu, M. *et al.* Integrated Lithium Niobate Modulator and Frequency Comb Generator Based on Fabry-Perot Resonators. in *Conference on Lasers and Electro-Optics JTh2B.27* (Optica Publishing Group, Washington, DC, 2020). doi:10.1364/CLEO_AT.2020.JTh2B.27.
101. Pan, B. *et al.* Compact electro-optic modulator on lithium niobate. *Photonics Res.* **10**, 697 (2022).
102. Pohl, D. *et al.* 100-GBd Waveguide Bragg Grating Modulator in Thin-Film Lithium Niobate. *IEEE Photonics Technol. Lett.* **33**, 85–88 (2021).
103. Xue, Y. *et al.* Breaking the bandwidth limit of a high-quality-factor ring modulator based on thin-film lithium niobate. *Optica* **9**, 1131 (2022).
104. Xu, M. *et al.* Michelson interferometer modulator based on hybrid silicon and lithium niobate platform. *APL Photonics* **4**, 100802 (2019).
105. Jian, J. *et al.* High modulation efficiency lithium niobate Michelson interferometer modulator. *Opt. Express* **27**, 18731 (2019).
106. Huang, X. *et al.* 40 GHz high-efficiency Michelson interferometer modulator on a silicon-rich nitride and thin-film lithium niobate hybrid platform. *Opt. Lett.* **46**, 2811 (2021).
107. Lin, Z. *et al.* High-performance polarization management devices based on thin-film lithium niobate. *Light Sci. Appl.* **11**, 93 (2022).
108. High-Efficiency, Slow-Light Modulator on Hybrid Thin-Film Lithium Niobate Platform | IEEE Journals & Magazine | IEEE Xplore. <https://ieeexplore.ieee.org/document/9520362>.
109. Parriaux, A., Hammani, K. & Millot, G. Electro-optic frequency combs. *Adv. Opt. Photonics* **12**, 223 (2020).
110. Beha, K. *et al.* Electronic synthesis of light. *Optica* **4**, 406 (2017).
111. Xu, M., He, M., Zhu, Y., Yu, S. & Cai, X. Flat Optical Frequency Comb Generator Based on Integrated Lithium Niobate Modulators. *J. Light. Technol.* **40**, 339–345 (2022).
112. Wang, K. *et al.* Generating arbitrary topological windings of a non-Hermitian band. *Science* **371**, 1240–1245 (2021).
113. Wang, K., Dutt, A., Wojcik, C. C. & Fan, S. Topological complex-energy braiding of non-Hermitian bands. *Nature* **598**, 59–64 (2021).
114. Ozawa, T., Price, H. M., Goldman, N., Zilberberg, O. & Carusotto, I. Synthetic dimensions in integrated photonics: From optical isolation to four-dimensional quantum Hall physics. *Phys. Rev. A* **93**, 043827 (2016).
115. Mittal, S., Goldschmidt, E. A. & Hafezi, M. A topological source of quantum light. *Nature* **561**, 502–506 (2018).

116. Wang, Z., Chong, Y., Joannopoulos, J. D. & Soljačić, M. Observation of unidirectional backscattering-immune topological electromagnetic states. *Nature* **461**, 772–775 (2009).
117. Fang, K., Yu, Z. & Fan, S. Realizing effective magnetic field for photons by controlling the phase of dynamic modulation. *Nat. Photonics* **6**, 782–787 (2012).
118. Bandres, M. A. *et al.* Topological insulator laser: Experiments. *Science* **359**, eaar4005 (2018).
119. Yuan, L., Xiao, M., Lin, Q. & Fan, S. Synthetic space with arbitrary dimensions in a few rings undergoing dynamic modulation. *Phys. Rev. B* **97**, 104105 (2018).
120. Yu, D. *et al.* Moiré Lattice in One-Dimensional Synthetic Frequency Dimension. *Phys. Rev. Lett.* **130**, 143801 (2023).
121. Cheng, D., Lustig, E., Wang, K. & Fan, S. Multi-dimensional band structure spectroscopy in the synthetic frequency dimension. *Light Sci. Appl.* **12**, 158 (2023).
122. Yu, D. *et al.* Simulating graphene dynamics in synthetic space with photonic rings. *Commun. Phys.* **4**, 219 (2021).
123. Rueda, A., Sedlmeir, F., Kumari, M., Leuchs, G. & Schwefel, H. G. L. Resonant electro-optic frequency comb. *Nature* **568**, 378–381 (2019).
124. Lukens, J. M. *et al.* All-Optical Frequency Processor for Networking Applications. *J. Light. Technol.* **38**, 1678–1687 (2020).
125. Supradeepa, V. R. *et al.* Comb-based radiofrequency photonic filters with rapid tunability and high selectivity. *Nat. Photonics* **6**, 186–194 (2012).
126. Fandiño, J. S., Muñoz, P., Doménech, D. & Capmany, J. A monolithic integrated photonic microwave filter. *Nat. Photonics* **11**, 124–129 (2017).
127. Zhu, X. *et al.* Hypercubic cluster states in the phase-modulated quantum optical frequency comb. *Optica* **8**, 281 (2021).
128. Lukens, J. M. & Lougovski, P. Frequency-encoded photonic qubits for scalable quantum information processing. *Optica* **4**, 8 (2017).
129. Lu, H.-H. *et al.* Quantum interference and correlation control of frequency-bin qubits. *Optica* **5**, 1455 (2018).
130. Kues, M. *et al.* Quantum optical microcombs. *Nat. Photonics* **13**, 170–179 (2019).
131. Menicucci, N. C., Flammia, S. T. & Pfister, O. One-Way Quantum Computing in the Optical Frequency Comb. *Phys. Rev. Lett.* **101**, 130501 (2008).
132. Kok, P. *et al.* Linear optical quantum computing with photonic qubits. *Rev. Mod. Phys.* **79**, 135–174 (2007).

133. Sinclair, N. *et al.* Spectral Multiplexing for Scalable Quantum Photonics using an Atomic Frequency Comb Quantum Memory and Feed-Forward Control. *Phys. Rev. Lett.* **113**, 053603 (2014).
134. Johnson, L. M. & Cox, C. H. Serrodyne optical frequency translation with high sideband suppression. *J. Light. Technol.* **6**, 109–112 (1988).
135. Wright, L. J., Karpiński, M., Söller, C. & Smith, B. J. Spectral Shearing of Quantum Light Pulses by Electro-Optic Phase Modulation. *Phys. Rev. Lett.* **118**, 023601 (2017).
136. Grimau Puigibert, M. *et al.* Heralded Single Photons Based on Spectral Multiplexing and Feed-Forward Control. *Phys. Rev. Lett.* **119**, 083601 (2017).
137. Youssefi, A. *et al.* A cryogenic electro-optic interconnect for superconducting devices. *Nat. Electron.* **4**, 326–332 (2021).
138. Tsang, M. Cavity quantum electro-optics. *Phys. Rev. A* **81**, 063837 (2010).
139. Tsang, M. Cavity quantum electro-optics. II. Input-output relations between traveling optical and microwave fields. *Phys. Rev. A* **84**, 043845 (2011).
140. Rueda, A. *et al.* Efficient microwave to optical photon conversion: an electro-optical realization. *Optica* **3**, 597 (2016).
141. Lambert, N. J., Rueda, A., Sedlmeir, F. & Schwefel, H. G. L. Coherent Conversion Between Microwave and Optical Photons—An Overview of Physical Implementations. *Adv. Quantum Technol.* **3**, 1900077 (2020).
142. Han, X., Fu, W., Zou, C.-L., Jiang, L. & Tang, H. X. Microwave-optical quantum frequency conversion. *Optica* **8**, 1050 (2021).
143. Xu, Y. *et al.* Light-Induced Dynamic Frequency Shifting of Microwave Photons in a Superconducting Electro-Optic Converter. *Phys. Rev. Appl.* **18**, 064045 (2022).
144. Krastanov, S. *et al.* Optically Heralded Entanglement of Superconducting Systems in Quantum Networks. *Phys. Rev. Lett.* **127**, 040503 (2021).
145. Warner, H. K. *et al.* Coherent control of a superconducting qubit using light. Preprint at <http://arxiv.org/abs/2310.16155> (2023).
146. Shen, M. *et al.* Photonic link from single flux quantum circuits to room temperature. Preprint at <http://arxiv.org/abs/2309.03284> (2023).
147. Shen, Y. *et al.* Deep learning with coherent nanophotonic circuits. *Nat. Photonics* **11**, 441–446 (2017).
148. Xu, X. *et al.* 11 TOPS photonic convolutional accelerator for optical neural networks. *Nature* **589**, 44–51 (2021).

149. Feldmann, J. *et al.* Parallel convolutional processing using an integrated photonic tensor core. *Nature* **589**, 52–58 (2021).
150. Ashtiani, F., Geers, A. J. & Aflatouni, F. An on-chip photonic deep neural network for image classification. *Nature* **606**, 501–506 (2022).
151. Pai, S. *et al.* Experimentally realized in situ backpropagation for deep learning in photonic neural networks. *Science* **380**, 398–404 (2023).
152. Chen, Z. *et al.* Deep learning with coherent VCSEL neural networks. *Nat. Photonics* **17**, 723–730 (2023).
153. Zhou, T. *et al.* Large-scale neuromorphic optoelectronic computing with a reconfigurable diffractive processing unit. *Nat. Photonics* **15**, 367–373 (2021).
154. Chen, Y. *et al.* Photonic unsupervised learning variational autoencoder for high-throughput and low-latency image transmission. *Sci. Adv.* **9**, eadf8437 (2023).
155. Liang, Y. *et al.* A high-gain cladded waveguide amplifier on erbium doped thin-film lithium niobate fabricated using photolithography assisted chemo-mechanical etching. *Nanophotonics* **11**, 1033–1040 (2022).
156. Zhou, J. *et al.* Laser diode-pumped compact hybrid lithium niobate microring laser. *Opt. Lett.* **47**, 5599 (2022).
157. Han, Y. *et al.* Electrically pumped widely tunable O-band hybrid lithium niobite/III-V laser. *Opt. Lett.* **46**, 5413 (2021).
158. Snigirev, V. *et al.* Ultrafast tunable lasers using lithium niobate integrated photonics. *Nature* **615**, 411–417 (2023).
159. Li, M. *et al.* Integrated Pockels laser. *Nat. Commun.* **13**, 5344 (2022).
160. Shams-Ansari, A. *et al.* Electrically pumped laser transmitter integrated on thin-film lithium niobate. *Optica* **9**, 408–411 (2022).
161. Shams-Ansari, A. Thin-film Lithium Niobate Laser Integration. in *Frontiers in Optics + Laser Science 2022 (FIO, LS) (2022)*, paper LM1F.4 LM1F.4 (Optica Publishing Group, 2022). doi:10.1364/LS.2022.LM1F.4.
162. Lufungula, I. L. *et al.* On-chip electro-optic frequency comb generation using a heterogeneously integrated laser. in *Conference on Lasers and Electro-Optics (2022)*, paper JTh6B.7 JTh6B.7 (Optica Publishing Group, 2022). doi:10.1364/CLEO_AT.2022.JTh6B.7.
163. Op De Beeck, C. *et al.* III/V-on-lithium niobate amplifiers and lasers. *Optica* **8**, 1288 (2021).
164. Zhang, X. *et al.* Heterogeneously integrated III–V-on-lithium niobate broadband light sources and photodetectors. *Opt. Lett.* **47**, 4564 (2022).
165. Zhang, X. *et al.* Heterogeneous integration of III–V semiconductor lasers on thin-film lithium niobite platform by wafer bonding. *Appl. Phys. Lett.* **122**, 081103 (2023).

166. Wang, C. *et al.* Monolithic lithium niobate photonic circuits for Kerr frequency comb generation and modulation. *Nat. Commun.* **10**, 978 (2019).
167. He, Y. *et al.* Self-starting bi-chromatic LiNbO₃ soliton microcomb. *Optica* **6**, 1138 (2019).
168. Gong, Z., Liu, X., Xu, Y. & Tang, H. X. Near-octave lithium niobate soliton microcomb. *Optica* **7**, 1275 (2020).
169. Guo, X. *et al.* High-performance modified uni-traveling carrier photodiode integrated on a thin-film lithium niobate platform. *Photonics Res.* **10**, 1338 (2022).
170. Wei, C. *et al.* Ultra-wideband Waveguide-coupled Photodiodes Heterogeneously Integrated on a Thin-film Lithium Niobate Platform. *Light Adv. Manuf.* **4**, 1 (2023).
171. O'Brien, J. L., Furusawa, A. & Vučković, J. Photonic quantum technologies. *Nat. Photonics* **3**, 687–695 (2009).
172. Lauk, N. *et al.* Perspectives on quantum transduction. *Quantum Sci. Technol.* **5**, 020501 (2020).
173. Wang, J., Sciarrino, F., Laing, A. & Thompson, M. G. Integrated photonic quantum technologies. *Nat. Photonics* **14**, 273–284 (2020).
174. Pelucchi, E. *et al.* The potential and global outlook of integrated photonics for quantum technologies. *Nat. Rev. Phys.* **4**, 194–208 (2022).
175. Moody, G. *et al.* 2022 Roadmap on integrated quantum photonics. *J. Phys. Photonics* **4**, 012501 (2022).
176. Lu, J., Li, M., Zou, C.-L., Al Sayem, A. & Tang, H. X. Toward 1% single-photon anharmonicity with periodically poled lithium niobate microring resonators. *Optica* **7**, 1654 (2020).
177. Chen, M., Menicucci, N. C. & Pfister, O. Experimental Realization of Multipartite Entanglement of 60 Modes of a Quantum Optical Frequency Comb. *Phys. Rev. Lett.* **112**, 120505 (2014).
178. Lu, H.-H., Simmerman, E. M., Lougovski, P., Weiner, A. M. & Lukens, J. M. Fully Arbitrary Control of Frequency-Bin Qubits. *Phys. Rev. Lett.* **125**, 120503 (2020).
179. Pfister, O. Continuous-variable quantum computing in the quantum optical frequency comb. *J. Phys. B At. Mol. Opt. Phys.* **53**, 012001 (2020).
180. Lu, H.-H., Lingaraju, N. B., Leaird, D. E., Weiner, A. M. & Lukens, J. M. High-dimensional discrete Fourier transform gates with a quantum frequency processor. *Opt. Express* **30**, 10126 (2022).
181. Lu, H.-H. *et al.* Bayesian tomography of high-dimensional on-chip biphoton frequency combs with randomized measurements. *Nat. Commun.* **13**, 4338 (2022).
182. Seshadri, S., Lu, H.-H., Leaird, D. E., Weiner, A. M. & Lukens, J. M. Complete Frequency-Bin Bell Basis Synthesizer. *Phys. Rev. Lett.* **129**, 230505 (2022).

183. Kues, M. *et al.* On-chip generation of high-dimensional entangled quantum states and their coherent control. *Nature* **546**, 622–626 (2017).
184. Yeh, M. *et al.* Single-photon frequency shifting using coupled microring resonators on thin-film lithium niobate. in *Conference on Lasers and Electro-Optics (2022)*, paper FTh5C.4 FTh5C.4 (Optica Publishing Group, 2022).
doi:10.1364/CLEO_QELS.2022.FTh5C.4.
185. Migdall, A. L., Branning, D. & Castelletto, S. Tailoring single-photon and multiphoton probabilities of a single-photon on-demand source. *Phys. Rev. A* **66**, 053805 (2002).
186. Nunn, J. *et al.* Enhancing Multiphoton Rates with Quantum Memories. *Phys. Rev. Lett.* **110**, 133601 (2013).
187. Xu, B.-Y. *et al.* Spectrally multiplexed and bright entangled photon pairs in a lithium niobate microresonator. *Sci. China Phys. Mech. Astron.* **65**, 294262 (2022).
188. Wolf, R. *et al.* Quasi-phase-matched nonlinear optical frequency conversion in on-chip whispering galleries. *Optica* **5**, 872 (2018).
189. Wang, X. *et al.* Quantum frequency conversion and single-photon detection with lithium niobate nanophotonic chips. *Npj Quantum Inf.* **9**, 38 (2023).
190. Roussev, R. V., Langrock, C., Kurz, J. R. & Fejer, M. M. Periodically poled lithium niobate waveguide sum-frequency generator for efficient single-photon detection at communication wavelengths. *Opt. Lett.* **29**, 1518 (2004).
191. Jankowski, M., Mishra, J. & Fejer, M. M. Dispersion-engineered $\chi(2)$ nanophotonics: a flexible tool for nonclassical light. *J. Phys. Photonics* **3**, 042005 (2021).
192. Ledezma, L. *et al.* Intense optical parametric amplification in dispersion-engineered nanophotonic lithium niobate waveguides. *Optica* **9**, 303 (2022).
193. Nehra, R. *et al.* Few-cycle vacuum squeezing in nanophotonics. *Science* **377**, 1333–1337 (2022).
194. Cui, C., Zhang, L. & Fan, L. In situ control of effective Kerr nonlinearity with Pockels integrated photonics. *Nat. Phys.* **18**, 497–501 (2022).
195. Shao, L. *et al.* Electrical control of surface acoustic waves. *Nat. Electron.* **5**, 348–355 (2022).
196. Wang, S. *et al.* Incorporation of erbium ions into thin-film lithium niobate integrated photonics. *Appl. Phys. Lett.* **116**, 151103 (2020).
197. Saglamyurek, E. *et al.* An integrated processor for photonic quantum states using a broadband light–matter interface. *New J. Phys.* **16**, 065019 (2014).
198. Zhang, X. *et al.* Symmetry-breaking-induced nonlinear optics at a microcavity surface. *Nat. Photonics* **13**, 21–24 (2019).

199. Tang, S.-J. *et al.* Single-particle photoacoustic vibrational spectroscopy using optical microresonators. *Nat. Photonics* (2023) doi:10.1038/s41566-023-01264-3.
200. Fang, K., Yu, Z. & Fan, S. Realizing effective magnetic field for photons by controlling the phase of dynamic modulation. *Nat. Photonics* **6**, 782–787 (2012).
201. Stokowski, H. S. *et al.* Integrated frequency-modulated optical parametric oscillator. Preprint at <http://arxiv.org/abs/2307.04200> (2023).
202. Englebert, N. *et al.* Bloch oscillations of coherently driven dissipative solitons in a synthetic dimension. *Nat. Phys.* (2023) doi:10.1038/s41567-023-02005-7.
203. Hwang, A. Y. *et al.* Mid-infrared spectroscopy with a broadly tunable thin-film lithium niobate optical parametric oscillator. *Optica* **10**, 1535 (2023).
204. Lei, F. *et al.* Self-injection-locked microcomb-based coherent oscillator. Preprint at <http://arxiv.org/abs/2310.08325> (2023).
205. Liu, J. *et al.* Photonic microwave generation in the X- and K-band using integrated soliton microcombs. *Nat. Photonics* **14**, 486–491 (2020).
206. Li, J., Yi, X., Lee, H., Diddams, S. A. & Vahala, K. J. Electro-optical frequency division and stable microwave synthesis. *Science* **345**, 309–313 (2014).
207. Tetsumoto, T. *et al.* Optically referenced 300 GHz millimetre-wave oscillator. *Nat. Photonics* **15**, 516–522 (2021).
208. Niu, R. *et al.* An integrated wavemeter based on fully-stabilized resonant electro-optic frequency comb. *Commun. Phys.* **6**, 329 (2023).
209. Niu, R. *et al.* kHz-precision wavemeter based on reconfigurable microsoliton. *Nat. Commun.* **14**, 169 (2023).
210. Spencer, D. T. *et al.* An optical-frequency synthesizer using integrated photonics. *Nature* **557**, 81–85 (2018).
211. Suh, M.-G. *et al.* Searching for exoplanets using a microresonator astrocomb. *Nat. Photonics* **13**, 25–30 (2019).
212. Obrzud, E. *et al.* A microphotonic astrocomb. *Nat. Photonics* **13**, 31–35 (2019).
213. Kim, I. *et al.* Nanophotonics for light detection and ranging technology. *Nat. Nanotechnol.* **16**, 508–524 (2021).
214. He, Y. *et al.* High-speed tunable microwave-rate soliton microcomb. *Nat. Commun.* **14**, 3467 (2023).
215. Cheng, R. *et al.* On-chip synchronous pumped c(3) optical parametric oscillator on thin-film lithium niobate.
216. Zhou, J. *et al.* On-Chip Integrated Waveguide Amplifiers on Erbium-Doped Thin-Film Lithium Niobate on Insulator. *Laser Photonics Rev.* **15**, 2100030 (2021).
217. Chen, Z. *et al.* Efficient erbium-doped thin-film lithium niobate waveguide amplifiers. *Opt. Lett.* **46**, 1161 (2021).
218. Luo, Q. *et al.* On-chip erbium-doped lithium niobate microring lasers. *Opt. Lett.* **46**, 3275 (2021).

219. Gaafar, M. A. *et al.* Femtosecond pulse amplification on a chip. Preprint at <http://arxiv.org/abs/2311.04758> (2023).
220. Guo, Q. *et al.* Ultrafast mode-locked laser in nanophotonic lithium niobate. *Science* **382**, 708–713 (2023).
221. Riemensberger, J. *et al.* A photonic integrated continuous-travelling-wave parametric amplifier. *Nature* **612**, 56–61 (2022).
222. Corato-Zanarella, M. *et al.* Widely tunable and narrow-linewidth chip-scale lasers from near-ultraviolet to near-infrared wavelengths. *Nat. Photonics* **17**, 157–164 (2023).
223. Dudley, J. M., Genty, G. & Coen, S. Supercontinuum generation in photonic crystal fiber. *Rev. Mod. Phys.* **78**, 1135–1184 (2006).
224. Zipfel, W. R., Williams, R. M. & Webb, W. W. Nonlinear magic: multiphoton microscopy in the biosciences. *Nat. Biotechnol.* **21**, 1369–1377 (2003).
225. Xue, X., Zheng, X. & Zhou, B. Super-efficient temporal solitons in mutually coupled optical cavities. *Nat. Photonics* **13**, 616–622 (2019).
226. Helgason, Ó. B. *et al.* Surpassing the nonlinear conversion efficiency of soliton microcombs. *Nat. Photonics* (2023) doi:10.1038/s41566-023-01280-3.
227. Zhao, Y., Jang, J. K., Okawachi, Y. & Gaeta, A. L. Theory of $\chi^{(2)}$ -microresonator-based frequency conversion. *Opt. Lett.* **46**, 5393 (2021).
228. Rabiei, P. & Gunter, P. Optical and electro-optical properties of submicrometer lithium niobate slab waveguides prepared by crystal ion slicing and wafer bonding. *Appl. Phys. Lett.* **85**, 4603–4605 (2004).
229. Rabiei, P. & Steier, W. H. Lithium niobate ridge waveguides and modulators fabricated using smart guide. *Appl. Phys. Lett.* **86**, 161115 (2005).
230. Hu, H., Gui, L., Ricken, R. & Sohler, W. Towards nonlinear photonic wires in lithium niobate. in *Integrated Optics: Devices, Materials, and Technologies XIV* vol. 7604 183–194 (SPIE, 2010).
231. Wang, J. *et al.* High-Q lithium niobate microdisk resonators on a chip for efficient electro-optic modulation. *Opt. Express* **23**, 23072–23078 (2015).
232. Wang, C. *et al.* Integrated high quality factor lithium niobate microdisk resonators. *Opt. Express* **22**, 30924 (2014).
233. Lin, J. *et al.* Fabrication of high-Q lithium niobate microresonators using femtosecond laser micromachining. *Sci. Rep.* **5**, 8072 (2015).
234. Wang, M. *et al.* On-chip electro-optic tuning of a lithium niobate microresonator with integrated in-plane microelectrodes. *Opt. Express* **25**, 124–129 (2017).

235. Fang, Z. *et al.* Monolithic integration of a lithium niobate microresonator with a free-standing waveguide using femtosecond laser assisted ion beam writing. *Sci. Rep.* **7**, 45610 (2017).
236. Lin, J. *et al.* Second harmonic generation in a high-Q lithium niobate microresonator fabricated by femtosecond laser micromachining. *Sci. China Phys. Mech. Astron.* **58**, 114209 (2015).
237. Lin, J. *et al.* Phase-Matched Second-Harmonic Generation in an On-Chip Lithium Niobate Microresonator. *Phys. Rev. Appl.* **6**, 014002 (2016).
238. Hao, Z. *et al.* Sum-frequency generation in on-chip lithium niobate microdisk resonators. *Photonics Res.* **5**, 623 (2017).
239. Liu, S., Zheng, Y. & Chen, X. Cascading second-order nonlinear processes in a lithium niobate-on-insulator microdisk. *Opt. Lett.* **42**, 3626 (2017).
240. Luo, R. *et al.* On-chip second-harmonic generation and broadband parametric down-conversion in a lithium niobate microresonator. *Opt. Express* **25**, 24531 (2017).
241. Lin, J. *et al.* Broadband Quasi-Phase-Matched Harmonic Generation in an On-Chip Monocrystalline Lithium Niobate Microdisk Resonator. *Phys. Rev. Lett.* **122**, 173903 (2019).
242. Liu, S. *et al.* Effective four-wave mixing in the lithium niobate on insulator microdisk by cascading quadratic processes. *Opt. Lett.* **44**, 1456 (2019).
243. Hao, Z. *et al.* Second-harmonic generation using d_{33} in periodically poled lithium niobate microdisk resonators. *Photonics Res.* **8**, 311 (2020).
244. Ye, X., Liu, S., Chen, Y., Zheng, Y. & Chen, X. Sum-frequency generation in lithium-niobate-on-insulator microdisk via modal phase matching. *Opt. Lett.* **45**, 523 (2020).
245. Zhang, L. *et al.* Dual-periodically poled lithium niobate microcavities supporting multiple coupled parametric processes. *Opt. Lett.* **45**, 3353 (2020).
246. Liang, H., Luo, R., He, Y., Jiang, H. & Lin, Q. High-quality lithium niobate photonic crystal nanocavities. *Optica* **4**, 1251–1258 (2017).
247. Jiang, H. *et al.* Nonlinear frequency conversion in one dimensional lithium niobate photonic crystal nanocavities. *Appl. Phys. Lett.* **113**, 021104 (2018).
248. Jiang, W. *et al.* Lithium niobate piezo-optomechanical crystals. *Optica* **6**, 845–853 (2019).
249. Jiang, W. *et al.* Efficient bidirectional piezo-optomechanical transduction between microwave and optical frequency. *Nat. Commun.* **11**, 1166 (2020).

250. High-Q 2D Lithium Niobate Photonic Crystal Slab Nanoresonators - Li - 2019 - Laser & Photonics Reviews - Wiley Online Library. <https://onlinelibrary.wiley.com/doi/10.1002/lpor.201800228>.
251. Xiang, T., Li, Y., Zheng, Y. & Chen, X. Multiple-DWDM-channel heralded single-photon source based on a periodically poled lithium niobate waveguide. *Opt. Express* **25**, 12493 (2017).
252. Xin, C. J. *et al.* Spectrally separable photon-pair generation in dispersion engineered thin-film lithium niobate. *Opt. Lett.* **47**, 2830 (2022).
253. Wang, L. *et al.* High-Q chaotic lithium niobate microdisk cavity. *Opt. Lett.* **43**, 2917–2920 (2018).
254. He, L. *et al.* Low-loss fiber-to-chip interface for lithium niobate photonic integrated circuits. *Opt. Lett.* **44**, 2314 (2019).
255. Shao, L. *et al.* Microwave-to-optical conversion using lithium niobate thin-film acoustic resonators. *Optica* **6**, 1498 (2019).
256. Pohl, D. *et al.* An integrated broadband spectrometer on thin-film lithium niobate. *Nat. Photonics* **14**, 24–29 (2020).
257. Luke, K. *et al.* Wafer-scale low-loss lithium niobate photonic integrated circuits. *Opt. Express* **28**, 24452 (2020).
258. Okawachi, Y. *et al.* Chip-based self-referencing using integrated lithium niobate waveguides. *Optica* **7**, 702 (2020).
259. Sayem, A. A., Cheng, R., Wang, S. & Tang, H. X. Lithium-niobate-on-insulator waveguide-integrated superconducting nanowire single-photon detectors. *Appl. Phys. Lett.* **116**, 151102 (2020).
260. Colangelo, M. *et al.* Superconducting nanowire single-photon detector on thin-film lithium niobate photonic waveguide. in *Conference on Lasers and Electro-Optics SM4O.4* (Optica Publishing Group, Washington, DC, 2020). doi:10.1364/CLEO_SI.2020.SM4O.4.
261. Lu, J. *et al.* Ultralow-threshold thin-film lithium niobate optical parametric oscillator. *Optica* **8**, 539 (2021).
262. McKenna, T. P. *et al.* Ultra-low-power second-order nonlinear optics on a chip. *Nat. Commun.* **13**, 4532 (2022).
263. Lomonte, E. *et al.* Single-photon detection and cryogenic reconfigurability in lithium niobate nanophotonic circuits. *Nat. Commun.* **12**, 6847 (2021).
264. Arrangoiz-Arriola, P. *et al.* Resolving the energy levels of a nanomechanical oscillator. *Nature* **571**, 537–540 (2019).
265. Guo, Q. *et al.* Femtojoule femtosecond all-optical switching in lithium niobate nanophotonics. *Nat. Photonics* **16**, 625–631 (2022).
266. Wollack, E. A. *et al.* Quantum state preparation and tomography of entangled mechanical resonators. *Nature* **604**, 463–467 (2022).

267. Shah, M., Briggs, I., Chen, P.-K., Hou, S. & Fan, L. Visible-telecom tunable dual-band optical isolator based on dynamic modulation in thin-film lithium niobate. *Opt. Lett.* **48**, 1978 (2023).
268. Yu, M. *et al.* Integrated electro-optic isolator on thin-film lithium niobate. *Nat. Photonics* (2023) doi:10.1038/s41566-023-01227-8.
269. Li, Z. *et al.* High density lithium niobate photonic integrated circuits. *Nat. Commun.* **14**, 4856 (2023).
270. Chen, P.-K. *et al.* Adapted poling to break the nonlinear efficiency limit in nanophotonic lithium niobate waveguides. *Nat. Nanotechnol.* (2023) doi:10.1038/s41565-023-01525-w.
271. Shang, C. *et al.* Inverse-Designed Lithium Niobate Nanophotonics. *ACS Photonics* acsphotonics.3c00040 (2023) doi:10.1021/acsphotonics.3c00040.